# Fragmentation contributions to hadroproduction of prompt $J/\psi$, $\chi_{cJ}$, and $\psi(2S)$ states

Geoffrey T. Bodwin,[1] Kuang-Ta Chao,[2,3,4] Hee Sok Chung,[1] U-Rae Kim,[5,6] Jungil Lee,[5] and Yan-Qing Ma[2,4]

[1]*High Energy Physics Division, Argonne National Laboratory, 9700 South Cass Avenue, Argonne, Illinois 60439, USA*

[2]*School of Physics and State Key Laboratory of Nuclear Physics and Technology, Peking University, Beijing 100871, China*

[3]*Center for High Energy Physics, Peking University, Beijing 100871, China*

[4]*Collaborative Innovation Center of Quantum Matter, Beijing 100871, China*

[5]*Department of Physics, Korea University, Seoul 136-701, Korea*

[6]*Korea Institute for Advanced Study, Seoul 130-722, Korea*

(Received 25 September 2015; published 29 February 2016)

We compute fragmentation corrections to hadroproduction of the quarkonium states $J/\psi$, $\chi_{cJ}$, and $\psi(2S)$ at leading power in $m_c^2/p_T^2$, where $m_c$ is the charm-quark mass and $p_T$ is the quarkonium transverse momentum. The computation is carried out in the framework of nonrelativistic QCD. We include corrections to the parton-production cross sections through next-to-leading order in the strong coupling $\alpha_s$ and corrections to the fragmentation functions through second order in $\alpha_s$. We also sum leading logarithms of $p_T^2/m_c^2$ to all orders in perturbation theory. We find that, when we combine these leading-power fragmentation corrections with fixed-order calculations through next-to-leading order in $\alpha_s$, we are able to obtain good fits for $p_T \geq 10$ GeV to hadroproduction cross sections that were measured at the Tevatron and the LHC. Using values for the nonperturbative long-distance matrix elements that we extract from the cross-section fits, we make predictions for the polarizations of the quarkonium states. We obtain good agreement with measurements of the polarizations, with the exception of the CDF Run II measurement of the prompt $J/\psi$ polarization, for which the agreement is only fair. In the predictions for the prompt-$J/\psi$ cross sections and polarizations, we take into account feeddown from the $\chi_{cJ}$ and $\psi(2S)$ states.

DOI: 10.1103/PhysRevD.93.034041

## I. INTRODUCTION

In recent years, corrections to inclusive quarkonium production cross sections and polarizations through next-to-leading order (NLO) in the strong coupling $\alpha_s$ have been computed for both hadroproduction [1–6] and photoproduction [7–9]. These computations have been carried out in the context of the nonrelativistic QCD (NRQCD) factorization conjecture [10], which states that the inclusive production cross section to produce a quarkonium $H$ in a collision of particles $A$ and $B$ can be written as

$$d\sigma_{A+B\to H+X} = \sum_n d\sigma_{A+B\to Q\bar{Q}(n)+X}\langle\mathcal{O}^H(n)\rangle. \qquad (1)$$

Here, the $d\sigma_{A+B\to Q\bar{Q}(n)+X}$ are the short-distance coefficients (SDCs), which can be computed in perturbation theory and which correspond to the production of a heavy quark-antiquark pair $Q\bar{Q}(n)$ in a specific color and angular-momentum state $n$. The $\langle\mathcal{O}^H(n)\rangle$ are NRQCD long-distance matrix elements (LDMEs), which parametrize the nonperturbative part of the production process.

Because the LDMEs have a known scaling with $v$, the heavy-quark velocity in the quarkonium rest frame [10], the sum in Eq. (1) can be regarded as an expansion in the small parameter $v$. ($v^2 \approx 0.3$ for the $J/\psi$.) In present-day phenomenology, the sum in Eq. (1) is truncated at relative order $v^4$. For $H = J/\psi$ or $H = \psi(2S)$, the truncated sum involves four LDMEs: $\langle\mathcal{O}^\psi({}^3S_1^{[1]})\rangle$, $\langle\mathcal{O}^\psi({}^3S_1^{[8]})\rangle$, $\langle\mathcal{O}^\psi({}^1S_0^{[8]})\rangle$, and $\langle\mathcal{O}^\psi({}^3P_J^{[8]})\rangle$, where the expressions in parentheses give the color state of the $Q\bar{Q}$ pair (singlet or octet) and spin and orbital angular momentum in spectroscopic notation. Here, $\psi$ stands for $J/\psi$ or $\psi(2S)$. For $H = \chi_{cJ}$, the truncated sum involves two LDMEs: $\langle\mathcal{O}^{\chi_{c0}}({}^3P_0^{[1]})\rangle$ and $\langle\mathcal{O}^{\chi_{c0}}({}^3S_1^{[8]})\rangle$, where the LDMEs for the $\chi_{c1}$ and $\chi_{c2}$ states can be related to the LDMEs for the $\chi_{c0}$ state by making use of the heavy-quark spin symmetry [10], which is valid up to corrections of relative order $v^2$.

Since the color-singlet LDME for quarkonium production $\langle\mathcal{O}^\psi({}^3S_1^{[1]})\rangle$ is related to the color-singlet LDME for quarkonium decay, it can be determined in lattice QCD, from potential models, or from the $\psi$ decay rates into lepton pairs. On the other hand, it is not known how to compute the color-octet production LDMEs from first principles, and they are usually fixed by comparisons of NRQCD factorization predictions with measured cross sections.

Even at the level of NLO accuracy in the theoretical predictions, it is not possible to achieve a fully consistent description of the existing $J/\psi$ production data within the NRQCD framework. For example, one can fit the

 

hadroproduction cross-section data [11,12] and polarization data [13–15] simultaneously [4], but the LDMEs that are obtained yield a prediction for the photoproduction cross section that is larger than the HERA data from the H1 Collaboration [16,17] by factors of 4–8 at the highest value of $p_T$ at which the cross section has been measured [18]. On the other hand, one can fit the predictions for the hadroproduction and photoproduction cross sections to the experimental data [5], but the LDMEs that are obtained lead to predictions of large transverse polarization in hadroproduction at large $p_T$, in disagreement with the experimental data [5]. In addition, it was found in Ref. [19] that the $\eta_c$ production data that were measured by the LHCb Collaboration [20] are incompatible with the LDMEs that were extracted in Ref. [5] from hadroproduction and photoproduction cross-section data. Although one can describe the $\eta_c$ production data by using the LDMEs that were extracted in Ref. [3], there is a very large cancellation between the contributions from the ${}^3S_1^{[8]}$ and ${}^3P_J^{[8]}$ channels [21,22], and, hence, the remainder may be strongly dependent on uncertainties from uncalculated higher-order contributions.

These difficulties provide motivation for calculations of quarkonium production cross sections beyond NLO accuracy in $\alpha_s$. An approach that simplifies computations beyond NLO in $\alpha_s$ is to compute rates at leading power (LP) or next-to-leading power (NLP) in $m_c^2/p_T^2$, where $m_c$ is the charm-quark mass and $p_T$ is the quarkonium transverse momentum. LP contributions can be factorized into semi-inclusive partonic cross sections to produce a specific single parton convolved with one-parton fragmentation functions (FFs) [23]. NLP contributions can be factorized into semi-inclusive partonic cross sections to produce two specific partons convolved with two-parton FFs [24]. Calculations of these fragmentation contributions, at any given order in $\alpha_s$, are much simpler than a full fixed-order calculation. Furthermore, the LP- and NLP-factorization frameworks are natural ones within which to resum large logarithms of $p_T^2/m_c^2$. Of course, because the LP and NLP contributions represent the leading and first subleading terms in an expansion in powers of $m_c^2/p_T^2$, one would not expect them to be valid unless $p_T$ is significantly greater than $m_c$.

In Ref. [25] it was found that LP contributions beyond NLO in $\alpha_s$ are important in $J/\psi$ hadroproduction. With the inclusion of these contributions, the LDMEs that are extracted from the prompt hadroproduction cross sections alone yield predictions for the $J/\psi$ polarization at large $p_T$ that are near zero and are in agreement with the experimental data [25]. One deficiency in the analysis of Ref. [25] is that it does not take into account the effects of feeddown from the $\chi_{cJ}$ and $\psi(2S)$ states to the $J/\psi$.

In this paper, we remedy that deficiency and extend the application of the LP-factorization approach by computing LP-fragmentation contributions to direct $J/\psi$, $\chi_{cJ}$, and $\psi(2S)$ production. We extract LDMEs by fitting to the Tevatron and LHC production cross sections, and we use those LDMEs to predict the $J/\psi$, $\chi_{cJ}$, and $\psi(2S)$ polarizations. Our predictions for the prompt $J/\psi$ and $\psi(2S)$ polarizations agree well with the existing high-$p_T$ LHC data, but the prompt $J/\psi$ polarization is in only fair agreement with the high-$p_T$ Tevatron Run II data. Our predictions for the $\chi_{cJ}$ polarizations will be tested soon at the LHC. While the results in this paper do not resolve the discrepancies between the NRQCD predictions and the $J/\psi$ photoproduction and $\eta_c$ hadroproduction data, they do provide a consistent description of the existing spin-triplet charmonium hadroproduction data at high $p_T$.

The remainder of this paper is organized as follows. In Sec. II, we discuss the form of the LP corrections that we compute. Section III contains the details of the calculation of the LP SDCs. We combine the LP and NLO results for the SDCs in Sec. IV. In Sec. V, we fit our predictions for the hadroproduction cross sections to the data, obtaining values for the LDMEs. We use these values for the LDMEs to make predictions for cross-section ratios and polarizations in Sec. VI. Finally, in Sec. VII, we summarize and discuss our results.

## II. CORRECTIONS TO QUARKONIUM PRODUCTION AT LEADING POWER IN $p_T$

The contribution of leading power in $p_T$ to a quarkonium production cross section is given by the LP-factorization formula [23]

$$d\sigma^{\rm LP}_{A+B\to Q\bar{Q}(n)+X}(p) = \int_0^1 dz \sum_i d\hat{\sigma}_{A+B\to i+X}(p_i = p/z, \mu_f) D_{i\to Q\bar{Q}(n)}(z,\mu_f). \tag{2}$$

Here, $d\hat{\sigma}_{A+B\to i+X}$ is the semi-inclusive parton-production cross section (PPCS) for hadrons $A$ and $B$ to produce parton $i$, and $D_{i\to Q\bar{Q}(n)}$ is the FF for parton $i$ to fragment into the $Q\bar{Q}$ pair with quantum numbers $n$. $p$ is the momentum of the $Q\bar{Q}$ pair, which is taken to be lightlike by neglecting the heavy-quark mass, and $p_i$ is the momentum of parton $i$, which is taken to be lightlike by neglecting the parton mass. $\mu_f$ is the factorization scale.

As we will describe in more detail in Sec. III, the PPCSs and the FFs have been calculated to order $\alpha_s^3$ and $\alpha_s^2$, respectively. Hence, we write them as

$$d\hat{\sigma}_{A+B\to i+X} = \alpha_s^2 d\hat{\sigma}^{(2)}_{A+B\to i+X} + \alpha_s^3 d\hat{\sigma}^{(3)}_{A+B\to i+X} + O(\alpha_s^4), \tag{3a}$$

$$D_{i\to Q\bar{Q}(n)} = \alpha_s D^{(1)}_{i\to Q\bar{Q}(n)} + \alpha_s^2 D^{(2)}_{i\to Q\bar{Q}(n)} + O(\alpha_s^3). \tag{3b}$$

As we have already mentioned, the SDCs for both unpolarized and polarized quarkonium production have been computed through NLO in $\alpha_s$, which is order $\alpha_s^4$. In this paper, we extend these order-$\alpha_s^4$ calculations by combining existing calculations of the PPCSs through order $\alpha_s^3$ and existing calculations of the FFs through order $\alpha_s^2$ to obtain a partial calculation of the order-$\alpha_s^5$ (NNLO) contributions to the LP SDCs. Furthermore, we calculate corrections to the LP SDCs involving leading logarithms of $p_T^2/m_c^2$ to all orders in $\alpha_s$ by solving the Dokshitzer-Gribov-Lipatov-Altarelli-Parisi (DGLAP) evolution equation [26–29]. Because this calculation of the LP SDCs accounts only partially for corrections of order $\alpha_s^5$, we expect uncertainties from uncalculated corrections to be of order $\alpha_s^5$. However, these uncalculated corrections will not contain any enhancements from leading logarithms of $p_T^2/m_c^2$.

Part of the LP-fragmentation contribution through order $\alpha_s^4$ is already included in the NLO SDCs, namely,

$$\begin{aligned} d\sigma_{\rm NLO}^{\rm LP}(p) &= \int_0^1 dz \sum_i \alpha_s^3 d\hat{\sigma}^{(2)}_{A+B\to i+X}(p_i = p/z, \mu_f) D^{(1)}_{i\to Q\bar{Q}(n)}(z,\mu_f) \\ &+ \int_0^1 dz \sum_i \alpha_s^4 [d\hat{\sigma}^{(2)}_{A+B\to i+X}(p_i = p/z, \mu_f) D^{(2)}_{i\to Q\bar{Q}(n)}(z,\mu_f) \\ &+ d\hat{\sigma}^{(3)}_{A+B\to i+X}(p_i = p/z, \mu_f) D^{(1)}_{i\to Q\bar{Q}(n)}(z,\mu_f)]. \end{aligned} \tag{4}$$

Hence, when we combine the SDCs through NLO in $\alpha_s$ and the LP-fragmentation contributions, we must subtract the contributions in Eq. (4) in order to avoid double counting. Following Ref. [25], we compute

$$\frac{d\sigma^{\rm LP+NLO}}{dp_T} = \frac{d\sigma^{\rm LP}}{dp_T} - \frac{d\sigma^{\rm LP}_{\rm NLO}}{dp_T} + \frac{d\sigma_{\rm NLO}}{dp_T}, \tag{5}$$

where $d\sigma_{\rm NLO}/dp_T$ is the SDC through NLO in $\alpha_s$. The expression (5) takes into account, without double counting, the complete calculations through NLO in $\alpha_s$ and also the additional LP corrections beyond NLO that we have mentioned.

## III. COMPUTATION OF THE LP SHORT-DISTANCE COEFFICIENTS

In this section we describe the details of the computation of the PPCSs and FFs that enter into the LP short-distance coefficients in the LP factorization formula (2).

We take $m_c = 1.5$ GeV. We use the CTEQ6M parton distribution functions and the two-loop expression for $\alpha_s$, with $n_f = 5$ quark flavors and $\Lambda^{(5)}_{\rm QCD} = 226$ MeV. We set the renormalization scale $\mu_r$ and the factorization scale $\mu_f$ for the both parton distribution functions and the FFs to be $m_T = \sqrt{p_T^2 + 4m_c^2}$. In order to resum leading logarithms of $p_T^2/m_c^2$, we evolve the FFs from the scale $\mu_0 = 2m_c$ to the scale $\mu_f = m_T \approx p_T$. We take the NRQCD factorization scale to be $\mu_\Lambda = m_c$. In the calculation of the PPCSs and the evolution of the FFs, we take $n_f = 3$ active-quark flavors. That is, we ignore contributions from virtual or initial heavy quarks.

### A. Parton production cross sections

The PPCSs through order $\alpha_s^3$ were computed in the modified minimal-subtraction ($\overline{\rm MS}$) scheme in Refs. [30,31]. We carry out numerical computations of the PPCSs through order $\alpha_s^3$ by making use of the computer code that was written by the authors of Ref. [30].

The PPCSs are computed as a function of $p_T$, $y$, and $z = p^+/p_i{}^+ = p_T/p_{iT}$, where $p_T$ is the transverse momentum of the $Q\bar{Q}$ pair, $y$ is the rapidity of the $Q\bar{Q}$ pair in the hadron center-of-momentum frame, and $p_{iT}$ is the transverse momentum of the specific parton that is produced in the semi-inclusive partonic scattering process. Here, we have written $z$ in terms of the transverse momenta by using the fact that, in the LP approximation, one can ignore the invariant mass of the $Q\bar{Q}$ pair. The maximum value of $p_{iT}$ is kinematically constrained, and, so, the PPCSs vanish for $z \le z_0 = \frac{p_T}{\sqrt{s}}(e^{+y} + e^{-y})$, where $\sqrt{s}$ is the center-of-mass energy.

### B. Fragmentation functions

In this paper we take into account FFs through order $\alpha_s^2$, which are available for fragmentation of both gluons and quarks into polarized and unpolarized $Q\bar{Q}$ pairs. A summary of FFs that we use in our calculation can be found in Ref. [32] and Ref. [33] for unpolarized and polarized $Q\bar{Q}$ pairs, respectively. We give a detailed description below of the sources of these FFs.

The gluon FF $D_{g\to Q\bar{Q}(n)}$ for $n = {}^3S_1^{[8]}$ was calculated for both unpolarized and polarized final states at order $\alpha_s$ (LO) in Ref. [34] and at order $\alpha_s^2$ (NLO) in Refs. [32,35]. The gluon FF for $n = {}^1S_0^{[8]}$ was calculated at order $\alpha_s^2$ (LO) in Refs. [36,37]. The gluon FFs for $n = {}^3P_J^{[8]}$ were calculated at order $\alpha_s^2$ (LO) in Refs. [34,37] for unpolarized final states and in Ref. [33] for polarized final states. The gluon FFs for $n = {}^3P_J^{[1]}$ were calculated at order $\alpha_s^2$ (LO) in Ref. [34] for unpolarized final states and in Refs. [33,38] for polarized final states.

The situation for quark FFs $D_{q\to Q\bar{Q}(n)}$ with $n$ an $S$-wave state is rather complicated, as there are several independent calculations, some of which do not agree. Let us distinguish three cases: (i) $q \neq Q$, in which case, $n = {}^3S_1^{[8]}$; (ii) $q = Q$ and $n = {}^3S_1^{[8]}$; (iii) $q = Q$ and $n = {}^3S_1^{[1]}$. The quark FF for case (i) for an unpolarized final state was calculated at order $\alpha_s^2$ (LO) in Refs. [32,39,40], whose results all agree. The quark FF for case (i) for a polarized final state was

calculated at order $\alpha_s^2$ (LO) in Refs. [33,39,41]. The results in Refs. [33,39] agree with each other, but disagree with the result in Ref. [41]. The results in Refs. [33,39] have since been confirmed by the author of Ref. [41]. The quark FF for case (ii) for an unpolarized final state was calculated at order $\alpha_s^2$ (LO) in Refs. [32,39,40,42]. The results in Refs. [32,39] agree with each other and disagree with the results in Refs. [40,42]. We use the results in Refs. [32,39] in this paper. The quark FF for case (ii) for a polarized final state was calculated at order $\alpha_s^2$ (LO) in Refs. [33,39,41], whose results agree. The quark FF for case (iii) for an unpolarized final state was calculated at order $\alpha_s^2$ (LO) in Refs. [32,39,43], whose results agree. The quark FF for case (iii) for a polarized final state was calculated at order $\alpha_s^2$ (LO) in Refs. [33,39,41], whose results agree.

The quark FFs $D_{Q\to Q\bar{Q}(n)}$ for $n = {}^3P_J^{[1]}$ and $n = {}^3P_J^{[8]}$ were calculated for the unpolarized and polarized cases at order $\alpha_s^2$ (LO) in Ref. [40].

The gluon FF $D_{g\to Q\bar{Q}({}^3S_1^{[1]})}$ was calculated at order $\alpha_s^3$ (LO) in Refs. [44,45]. Because the contributions to the FF in the ${}^3S_1^{[1]}$ channel begin at order $\alpha_s^3$, we do not include them in our LP-fragmentation calculations. However, we do use the LO FF for the ${}^3S_1^{[1]}$ channel to estimate the size of the uncalculated LP-fragmentation contributions for that channel.

### C. DGLAP equation

At leading order in $\alpha_s$, the DGLAP equation is given by [26–29]

$$\frac{d}{d\log\mu_f^2}\begin{pmatrix} D_S(\mu_f) \\ D_g(\mu_f)\end{pmatrix} = \frac{\alpha_s(\mu_f)}{2\pi}\begin{pmatrix} P_{qq} & 2n_f P_{gq} \\ P_{qg} & P_{gg}\end{pmatrix} \otimes \begin{pmatrix} D_S(\mu_f) \\ D_g(\mu_f)\end{pmatrix}, \tag{6}$$

where $D_g = D_{g\to Q\bar{Q}(n)}$, $D_S = \sum_f [D_{q_f\to Q\bar{Q}(n)} + D_{\bar{q}_f\to Q\bar{Q}(n)}]$, $f$ is the light-quark or light-antiquark flavor, the $P_{ij}$ are the splitting functions for the FFs, and $n_f$ is the number of active light-quark flavors. The symbol $\otimes$ represents the convolution

$$\begin{aligned}(f\otimes g)(z) &= \int_0^1 dx \int_0^1 dy f(x)g(y)\delta(xy-z) \\ &= \int_z^1 \frac{dx}{x} f(z/x)g(x) \\ &= \int_z^1 \frac{dx}{x} f(x)g(z/x).\end{aligned} \tag{7}$$

The splitting functions are given by

$$P_{gg}(z) = 2C_A\left[\frac{z}{(1-z)_+} + \frac{1-z}{z} + z(1-z) + \frac{b_0}{12}\delta(1-z)\right], \tag{8a}$$

$$P_{gq}(z) = C_F\frac{1+(1-z)^2}{z}, \tag{8b}$$

$$P_{qg}(z) = T_F[z^2+(1-z)^2], \tag{8c}$$

$$P_{qq}(z) = C_F\left[\frac{1+z^2}{(1-z)_+} + \frac{3}{2}\delta(1-z)\right], \tag{8d}$$

where

$$C_A = N_c, \tag{9a}$$

$$C_F = \frac{N_c^2-1}{2N_c}, \tag{9b}$$

$$T_F = \frac{1}{2}, \tag{9c}$$

$$b_0 = \frac{11}{3}N_c - \frac{2}{3}n_f, \tag{9d}$$

and $N_c = 3$ is the number of colors.

As is well known, an analytic solution to Eq. (6) can be obtained in Mellin space. The Mellin transform of a function $f$ is defined by

$$\tilde{f}(N) = (\mathcal{M}f)(N) = \int_0^1 dz\, z^{N-1} f(z), \tag{10}$$

where we use a tilde ($\tilde{}$) to denote objects in Mellin space. The Mellin transform of the convolution in Eq. (6) is an ordinary product:

$$[\mathcal{M}(f\otimes g)](N) = (\mathcal{M}f)(N)\times(\mathcal{M}g)(N). \tag{11}$$

Hence, Eq. (6) can be diagonalized by taking the Mellin transform. Using the one-loop evolution of $\alpha_s$

$$\frac{d}{d\log\mu_f^2} = -\frac{b_0}{4\pi}\alpha_s^2(\mu_f)\frac{d}{d\alpha_s(\mu_f)}, \tag{12}$$

one obtains the following solution of the DGLAP equation:

$$\begin{pmatrix} \tilde{D}_S(N,\mu_f) \\ \tilde{D}_g(N,\mu_f) \end{pmatrix} = \left[ M_+ \left( \frac{\alpha_s(\mu_0)}{\alpha_s(\mu_f)} \right)^{2\tilde{P}^+/b_0} + M_- \left( \frac{\alpha_s(\mu_0)}{\alpha_s(\mu_f)} \right)^{2\tilde{P}^-/b_0} \right] \times \begin{pmatrix} \tilde{D}_S(N,\mu_0) \\ \tilde{D}_g(N,\mu_0) \end{pmatrix}, \quad (13)$$

where

$$M_\pm = \pm \frac{1}{\tilde{P}^+ - \tilde{P}^-} \begin{pmatrix} \tilde{P}_{qq} - \tilde{P}^\mp & 2n_f \tilde{P}_{gq} \\ \tilde{P}_{qg} & \tilde{P}_{gg} - \tilde{P}^\mp \end{pmatrix}, \quad (14)$$

and

$$\tilde{P}^\pm = \frac{1}{2} \left[ \tilde{P}_{gg} + \tilde{P}_{qq} \pm \sqrt{(\tilde{P}_{gg} - \tilde{P}_{qq})^2 + 8n_f \tilde{P}_{qg} \tilde{P}_{gq}} \right]. \quad (15)$$

The evolved FFs in $z$-space can be obtained from Eq. (13) by applying the inverse Mellin transform

$$D_{i\to Q\bar{Q}(n)}(z,\mu_f) = \frac{1}{2\pi i} \int_{c-i\infty}^{c+i\infty} dN z^{-N} \tilde{D}_{i\to Q\bar{Q}(n)}(N,\mu_f), \quad (16)$$

where the real number $c$ is chosen so that the integral over $N$ follows a contour that lies to the right of all of the poles of $\tilde{D}_{i\to Q\bar{Q}(n)}(N,\mu_f)$.

We resum the leading logarithms of $p_T^2/m_c^2$ by choosing the evolution scales $\mu_0 = 2m_c$ and $\mu_f = m_T \approx p_T$. In this paper, we compute the integral over $N$ numerically, using analytic expressions for the Mellin transforms of the FFs at the scale $\mu_0 = 2m_c$.

There is a difficulty in numerical computation of the inverse Mellin transform in Eq. (16) near $z = 1$. For $z \ll 1$, the factor $z^{-N}$ causes the integrand to vanish quickly at large $|N|$ and the integral over $N$ converges. On the other hand, when $z = 1$, the convergence of the integral depends solely on the behavior of the Mellin-space FF $\tilde{D}_{i\to Q\bar{Q}(n)}(N,\mu_f)$ at large $|N|$. Since $\tilde{P}_{gg}$ and $\tilde{P}_{qq}$ behave asymptotically as negative constants times $\log|N|$, while $\tilde{P}_{gq}$ and $\tilde{P}_{qg}$ vanish asymptotically as inverse powers of $N$, the coefficients of $M_+$ and $M_-$ in Eq. (16) damp the integral when $\alpha_s(\mu_f) \ll \alpha_s(\mu_0)$. However, the integrals do not converge at $z = 1$ unless $\mu_f$ is quite large in comparison with $\mu_0$. In fact, as $\mu_f$ approaches $\mu_0$, the evolved FFs approximate the initial FFs, which, in some cases, are distributions at $z = 1$. We deal with this problem by rearranging the convolutions of the FFs and the PPCSs so as to treat the singular behavior of the FFs at $z = 1$ analytically. The details of the method are given in the Appendix.

## IV. RESULTS FOR COMBINED LP AND NLO SHORT-DISTANCE COEFFICIENTS

Now we use Eq. (5) to combine results for the LP SDCs, computed as described in Sec. III, with the SDCs through NLO in $\alpha_s$. For the latter, we make use of the computations in Refs. [1,3,4], taking the values of the parton distributions, $m_c$, $\alpha_s$, $\mu_r$, $\mu_f$, $\mu_\Lambda$, and $n_f$ that are specified at the start of Sec. III.[1]

We first compare our results for $d\sigma_{\rm NLO}^{\rm LP}/dp_T$ with $d\sigma_{\rm NLO}/dp_T$, the fixed-order SDC accurate through NLO. Figures 1–4 show the ratios $(d\sigma_{\rm NLO}^{\rm LP}/dp_T)/(d\sigma_{\rm NLO}/dp_T)$ for the polarized and unpolarized final states in the process $pp \to H + X$ at $\sqrt{s} = 7$ TeV and $|y| < 1.2$.

In Fig. 1, we show the ratios $(d\sigma_{\rm NLO}^{\rm LP}/dp_T)/(d\sigma_{\rm NLO}/dp_T)$ for unpolarized final states in the ${}^3S_1^{[8]}$, ${}^1S_0^{[8]}$, and ${}^3P_J^{[8]}$ channels. As $p_T$ increases, the ratios for the ${}^3S_1^{[8]}$ and ${}^3P_J^{[8]}$ channels quickly approach unity because the LP-fragmentation contribution dominates the SDCs. This approach to unity is slower for the ${}^1S_0^{[8]}$ channel because the FF for the ${}^1S_0^{[8]}$ channel does not receive enhancements near $z = 1$ from a Dirac $\delta$ function or plus distributions that are the remnants of soft divergences that cancel between real and virtual gluon-emission processes.[2] At small $p_T$, the ratio $(d\sigma_{\rm NLO}^{\rm LP}/dp_T)/(d\sigma_{\rm NLO}/dp_T)$ is larger

[1] In order to improve computational efficiency, we have omitted in the calculation of $d\sigma_{\rm NLO}/dp_T$ contributions from processes that are initiated by two light quarks, two light-antiquarks, or a light quark and a light antiquark, where the two initial partons can have different flavors. We use the generic expression $qq$ to denote these light-quark/antiquark initial states. The $qq$-initiated contributions are small in comparison to the sum of the $qg$- and $gg$-initiated contributions because the $q$ and $\bar{q}$ partonic fluxes are small in comparison to the $g$ partonic flux. As $p_T$ increases, the sizes of the $q$ and $\bar{q}$ partonic fluxes increase relative to the size of the $g$ partonic flux because larger values of the parton momentum fractions are emphasized. At large values of $p_T$, $d\sigma_{\rm NLO}/dp_T$ is well approximated by $d\sigma_{\rm NLO}^{\rm LP}/dp_T$. Therefore, we adopt the following computational strategy. In order to match what was done in the NLO calculation, we omit the $qq$-initiated contributions in computing $d\sigma_{\rm NLO}^{\rm LP}/dp_T$ in Eq. (5). However, we take the $qq$-initiated contributions into account at large $p_T$, where they can be more important, by including them in the computation of $d\sigma^{\rm LP}/dp_T$ in Eq. (5). Since each $qq$-initiated process that produces a given $Q\bar{Q}$ channel contains an LP fragmentation contribution at the leading nontrivial order in $\alpha_s$, we can use LP fragmentation results to estimate the sizes of the $qq$-initiated contributions. These estimates indicate that $qq$-initiated contributions produce the largest fractional correction in the longitudinally polarized ${}^3S_1^{[8]}$ channel, in which they grow to about 5% of the total at $p_T = 100$ GeV. Hence, we expect any errors that result from the omission of the $qq$-initiated processes in the NLO calculations to be much less than 5%.

[2] It was shown in Ref. [46] that the ratio $(d\sigma_{\rm NLO}^{\rm LP}/dp_T + d\sigma_{\rm NLO}^{\rm NLP}/dp_T)/(d\sigma_{\rm NLO}/dp_T)$, which takes into account both the LP and NLP contributions, approaches unity much faster for the ${}^1S_0^{[8]}$ channel than does the ratio $(d\sigma_{\rm NLO}^{\rm LP}/dp_T)/(d\sigma_{\rm NLO}/dp_T)$.

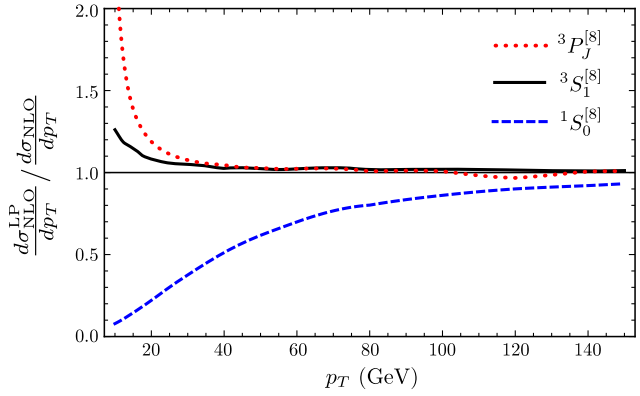


FIG. 1. The ratio $(d\sigma_{\rm NLO}^{\rm LP}/dp_T)/(d\sigma_{\rm NLO}/dp_T)$ for the $^1S_0^{[8]}$, $^3P_J^{[8]}$, and $^3S_1^{[8]}$ channels in the process $pp \to H + X$ at $\sqrt{s} = 7$ TeV and $|y| < 1.2$.

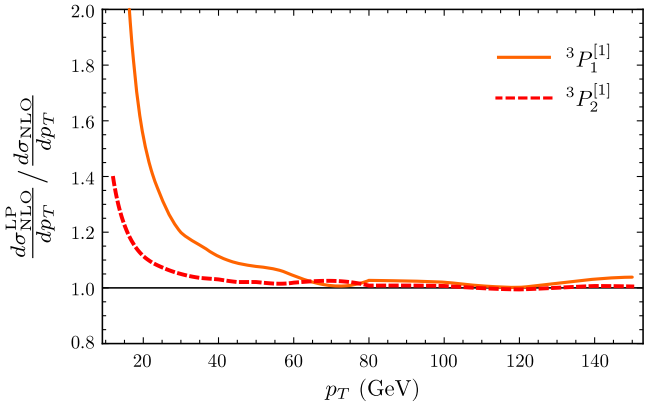


FIG. 3. The ratio $(d\sigma_{\rm NLO}^{\rm LP}/dp_T)/(d\sigma_{\rm NLO}/dp_T)$ for the $^3P_1^{[1]}$ and $^3P_2^{[1]}$ channels in the process $pp \to H + X$ at $\sqrt{s} = 7$ TeV and $|y| < 1.2$.

for the $^3P_J^{[8]}$ channel than for the $^3S_1^{[8]}$ and $^1S_0^{[8]}$ channels because, for the $^3P_J^{[8]}$ channel, the LO and NLO contributions in the denominator tend to cancel.

In Fig. 2, we show the ratios $(d\sigma_{\rm NLO}^{\rm LP}/dp_T)/(d\sigma_{\rm NLO}/dp_T)$ for longitudinal final states in the $^3S_1^{[8]}$ and $^3P_J^{[8]}$ channels. The approach of each of these ratios to unity is slow. As was the case for the ratio of cross sections in the $^1S_0^{[8]}$ channel, the slow approach to unity is a consequence of the fact that the FFs are not enhanced near $z = 1$ by a Dirac $\delta$ function or plus distributions.

In Fig. 3, we show the ratios $(d\sigma_{\rm NLO}^{\rm LP}/dp_T)/(d\sigma_{\rm NLO}/dp_T)$ for unpolarized final states in the color-singlet $P$-wave channels. We show the ratios for the polarized final states in Fig. 4. Here, $h$ is the helicity of the $Q\bar{Q}$ pair in the final state. The behaviors are similar to those for the $^3P_J^{[8]}$ channel, except for the case of $J = 2$ with $|h| = 1$, for which the ratio $(d\sigma_{\rm NLO}^{\rm LP}/dp_T)/(d\sigma_{\rm NLO}/dp_T)$ is almost constant. We note that the deviation of $(d\sigma_{\rm NLO}^{\rm LP}/dp_T)/(d\sigma_{\rm NLO}/dp_T)$ from unity at large $p_T$ is of the same relative size as the statistical uncertainty in the NLO calculation.

Next we compare $d\sigma_{\rm NLO}^{\rm LP+NLO}/dp_T$, the SDC that includes both the fixed-order corrections through NLO and the additional LP corrections, with $d\sigma_{\rm NLO}/dp_T$, the SDC that includes fixed-order corrections through NLO. Specifically, we show the ratios $(d\sigma_{\rm NLO}^{\rm LP+NLO}/dp_T)/(d\sigma_{\rm NLO}/dp_T)$ for the polarized and unpolarized final states in Figs. 5–8. With the exception of the $^3S_1^{[8]}$ channel, the additional LP-fragmentation contributions are of the order of 100% at large $p_T$. As we have mentioned, because there is a partial cancellation between the LO and the NLO contributions in the $^3P_J^{[8]}$ channel, the additional LP fragmentation corrections have a significant impact on the shape in that channel. For the $^3S_1^{[8]}$ channel the additional LP-fragmentation contributions are negative and only mildly alter the shape.

As was pointed out in Ref. [25], the effects from the all-orders resummation of logarithms of $p_T^2/m_c^2$ are small.

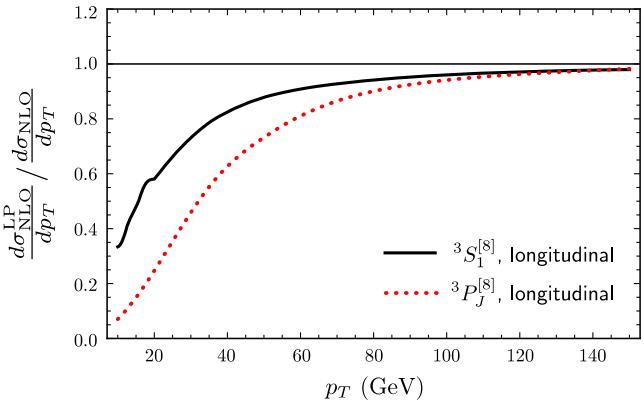


FIG. 2. The ratio $(d\sigma_{\rm NLO}^{\rm LP}/dp_T)/(d\sigma_{\rm NLO}/dp_T)$ for the polarized $^3P_J^{[8]}$ and $^3S_1^{[8]}$ channels with longitudinal final states in the process $pp \to H + X$ at $\sqrt{s} = 7$ TeV and $|y| < 1.2$.

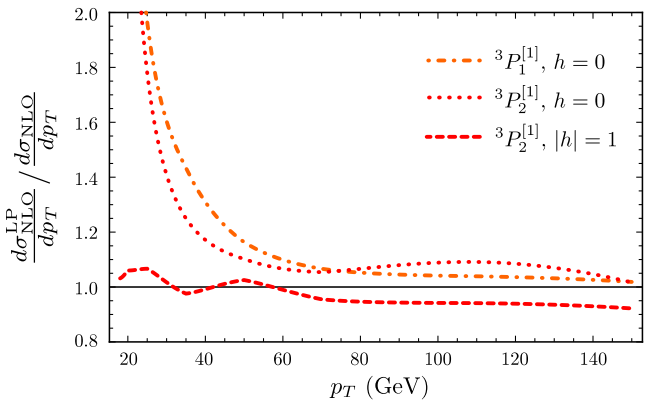


FIG. 4. The ratio $(d\sigma_{\rm NLO}^{\rm LP}/dp_T)/(d\sigma_{\rm NLO}/dp_T)$ for the polarized $^3P_1^{[1]}$ and $^3P_2^{[1]}$ channels in the process $pp \to H + X$ at $\sqrt{s} = 7$ TeV and $|y| < 1.2$. $h$ is the helicity of the $Q\bar{Q}$ pair in the final state.

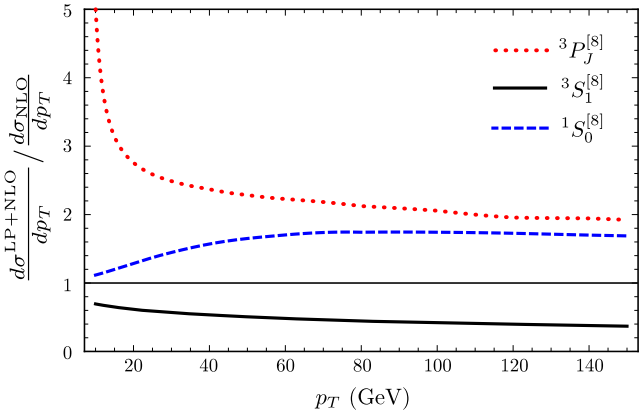


FIG. 5. The ratio $(d\sigma^{\mathrm{LP+NLO}}/dp_T)/(d\sigma_{\mathrm{NLO}}/dp_T)$ for the $^1S_0^{[8]}$, $^3P_J^{[8]}$, and $^3S_1^{[8]}$ channels with unpolarized final states in the process $pp \to H + X$ at $\sqrt{s} = 7$ TeV and $|y| < 1.2$.

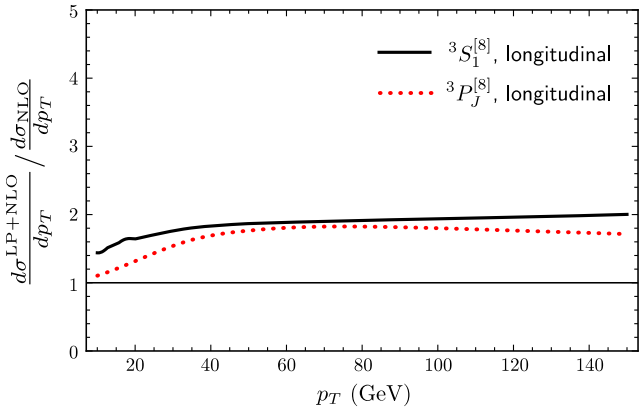


FIG. 6. The ratio $(d\sigma^{\mathrm{LP+NLO}}/dp_T)/(d\sigma_{\mathrm{NLO}}/dp_T)$ for the polarized $^3P_J^{[8]}$ and $^3S_1^{[8]}$ channels with longitudinal final states in the process $pp \to H + X$ at $\sqrt{s} = 7$ TeV and $|y| < 1.2$.

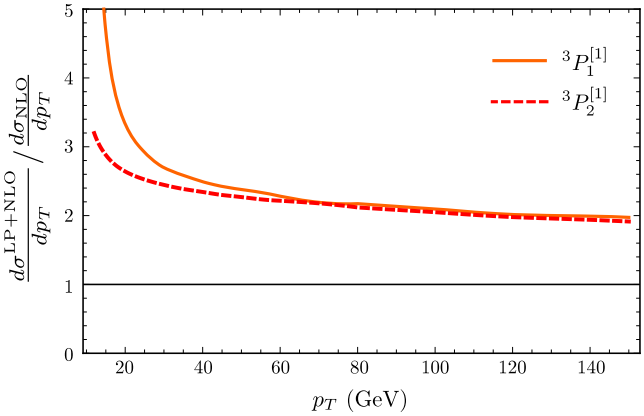


FIG. 7. The ratio $(d\sigma^{\mathrm{LP+NLO}}/dp_T)/(d\sigma_{\mathrm{NLO}}/dp_T)$ for the $^3P_1^{[1]}$ and $^3P_2^{[1]}$ channels with unpolarized final states in the process $pp \to H + X$ at $\sqrt{s} = 7$ TeV and $|y| < 1.2$.

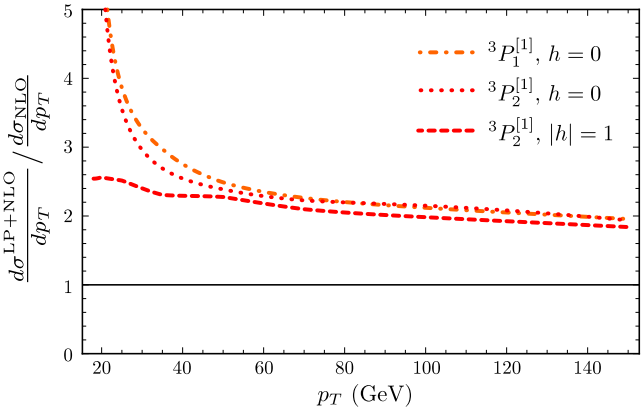


FIG. 8. The ratio $(d\sigma^{\mathrm{LP+NLO}}/dp_T)/(d\sigma_{\mathrm{NLO}}/dp_T)$ for the $^3P_1^{[1]}$ and $^3P_2^{[1]}$ channels with polarized final states in the process $pp \to H + X$ at $\sqrt{s} = 7$ TeV and $|y| < 1.2$.

In the case of the $^3S_1^{[8]}$ channel, almost all of the effects of the large logarithms are already accounted for in the NLO contribution. In the cases of the $^1S_0^{[8]}$ and $^3P_J^{[8]}$ channels, the all-orders resummations of logarithms shift the FFs by only about 2% and 5%, respectively, at $p_T = 52.7$ GeV because contributions from the running of $\alpha_s$ and from the DGLAP splitting cancel. Hence, almost all of the large additional LP corrections that we find arise from nonlogarithmic contributions of order $\alpha_s^5$.

Finally, we discuss the LP-fragmentation contribution to the $^3S_1^{[1]}$ channel. Since the FF for this channel begins at order $\alpha_s^3$, the $^3S_1^{[1]}$ channel receives an LP contribution that begins at order $\alpha_s^5$ (NNLO). We do not include this LP-fragmentation contribution in our analysis. However, we have estimated its size by making use of the FF at order $\alpha_s^3$. At $p_T = 10$ GeV, the LP contribution is about an order of magnitude smaller than the fixed-order contribution through NLO. The LP contribution reaches the same size as the fixed-order contribution through NLO at around $p_T = 50$ GeV. Finally, when $p_T = 130$ GeV, the LP contribution is almost an order of magnitude larger than the fixed-order contribution through NLO. Although the LP-fragmentation contribution can have a significant effect on the color-singlet contribution at large $p_T$, its effect on the cross section is only of the order of 1% of the measured cross section at $p_T = 130$ GeV.

## V. FITS OF CROSS-SECTION PREDICTIONS TO DATA

In this section we extract the color-octet LDMEs by fitting the cross-section predictions that are based on the LP + NLO SDCs to the measured cross sections. We use the resulting LDMEs to make predictions for the prompt-$J/\psi$ polarization. In order to suppress possible nonfactorizing contributions, we fit only to data for which $p_T$ is

greater than $3m_H$, where $m_H$ is the quarkonium mass. Since the shape of the $p_T$ distribution determines the LDMEs, it is crucial to use the data at the highest $p_T$ values in the fits.

In the case of the direct $J/\psi$ cross section, we estimate the theoretical uncertainties in the SDCs to be 25% of the central values. We arrived at these uncertainties by varying the factorization scale $\mu_f$ and the renormalization scale $\mu_r$ independently between $\frac{1}{2}m_T$ and $2m_T$. This 25% uncertainty is also roughly the size of the uncertainty that one would expect from uncalculated corrections of higher order in $v$. In the cases of the cross sections of the excited charmonium states, we take the uncertainties to be 30% of the central values because the $v^2$ for those states is larger than for the $J/\psi$.

### A. Production of $\psi(2S)$

We determine the three color-octet $\psi(2S)$ LDMEs by performing a least-$\chi^2$ fit to the CDF [47] and CMS [12,48] cross-section data. In order to suppress possible nonfactorizing contributions, we use only the data for which $p_T$ is greater than 11 GeV. We ignore feeddown contributions from decays of heavier quarkonia.

In the case of the color-singlet LDME, we take a value that was determined in a potential-model calculation [49]: $\langle \mathcal{O}^{\psi(2S)}({}^3S_1^{[1]})\rangle = 0.76\ \mathrm{GeV}^3$. Different choices for the value of the color-singlet LDME would have little effect on our results, as the contribution from the color-singlet channel is much smaller than the theoretical uncertainties. In the lowest $p_T$ bin that we consider for the CMS data that have $|y| < 1.2$ (11 GeV $< p_T <$ 12 GeV), the contribution from the color-singlet channel is only about 5% of the cross section, and the color-singlet contribution drops to 0.2% in the highest $p_T$ bin (75 GeV $< p_T <$ 100 GeV).

The fitted LP + NLO cross section is compared with the data in Fig. 9. The quality of the fit is quite good, with $\chi^2/\mathrm{d.o.f.} = 1.71/29$. As can be seen from Fig. 10, the cross section is dominated by the ${}^1S_0^{[8]}$ channel at moderate values of $p_T$, but not at large values of $p_T$. The concept of ${}^1S_0^{[8]}$ dominance has been suggested previously in Refs. [4,25,50].

The color-octet LDMEs that are obtained from the fit are

$$\langle \mathcal{O}^{\psi(2S)}({}^3S_1^{[8]})\rangle = (-1.57 \pm 2.80) \times 10^{-3}\ \mathrm{GeV}^3, \quad (17a)$$

$$\langle \mathcal{O}^{\psi(2S)}({}^1S_0^{[8]})\rangle = (+3.14 \pm 0.79) \times 10^{-2}\ \mathrm{GeV}^3, \quad (17b)$$

$$\frac{\langle \mathcal{O}^{\psi(2S)}({}^3P_0^{[8]})\rangle}{m_c^2} = (-1.14 \pm 1.21) \times 10^{-3}\ \mathrm{GeV}^3. \quad (17c)$$

The uncertainties that are shown above are correlated. The correlation matrix of the uncertainties in $\langle \mathcal{O}^{\psi(2S)}({}^3S_1^{[8]})\rangle$, $\langle \mathcal{O}^{\psi(2S)}({}^1S_0^{[8]})\rangle$, and $\langle \mathcal{O}^{\psi(2S)}({}^3P_0^{[8]})\rangle/m_c^2$, respectively, is

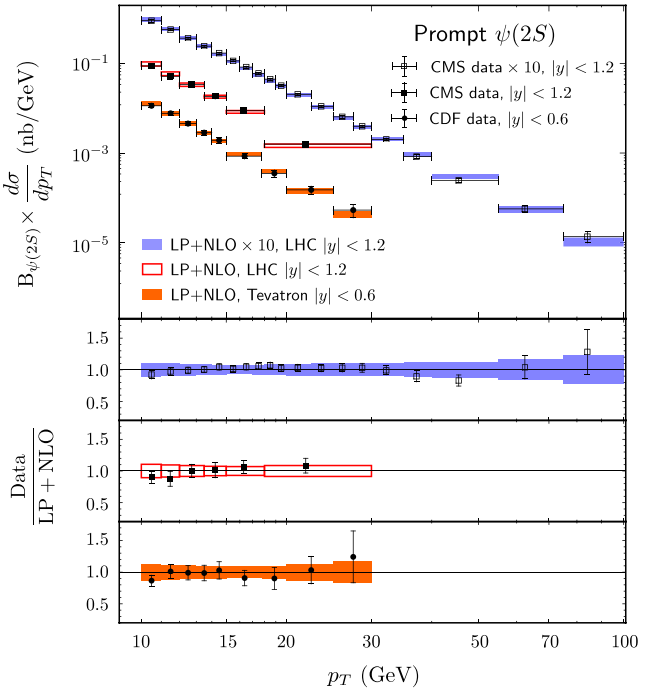


FIG. 9. The differential cross sections for prompt $\psi(2S)$ production at the Tevatron ($\sqrt{s} = 1.96\,\mathrm{TeV}$) and the LHC ($\sqrt{s} = 7\,\mathrm{TeV}$). $B_{\psi(2S)} = \mathrm{Br}[\psi(2S) \to \mu^+\mu^-]$, where Br denotes a branching ratio.

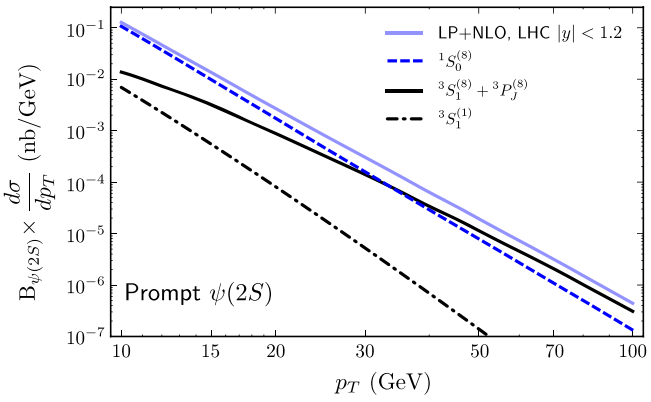


FIG. 10. Contributions of the individual channels to the prompt $\psi(2S)$ differential cross section at the LHC ($\sqrt{s} = 7\,\mathrm{TeV}$). $B_{\psi(2S)} = \mathrm{Br}[\psi(2S) \to \mu^+\mu^-]$.

$$C^{\psi(2S)} = \begin{pmatrix} 7.85 & -14.7 & 3.36 \\ -14.7 & 62.2 & -5.52 \\ 3.36 & -5.52 & 1.46 \end{pmatrix} \times 10^{-6}\ \mathrm{GeV}^6. \quad (18)$$

It is useful to examine the correlation matrix of relative uncertainties, $\bar{C}^{\psi(2S)}$, whose components are defined by

$$\bar{C}^{\psi(2S)}_{mn} = \frac{C^{\psi(2S)}_{mn}}{\mathcal{O}_n \mathcal{O}_m}, \quad (19)$$

where $\mathcal{O}_n$ is the central value of the $n$th LDME. Then $\bar{C}^{\psi(2S)}$ is given by

$$\bar{C}^{\psi(2S)} = \begin{pmatrix} 32.0 & 2.98 & 18.9 \\ 2.98 & 0.63 & 1.55 \\ 18.9 & 1.55 & 11.3 \end{pmatrix} \times 10^{-1}. \quad (20)$$

The normalized eigenvectors of $\bar{C}^{\psi(2S)}$ are

$$v_1^{\psi(2S)} = \begin{pmatrix} 0.858 \\ 0.0780 \\ 0.508 \end{pmatrix}, \quad v_2^{\psi(2S)} = \begin{pmatrix} 0.181 \\ 0.879 \\ -0.441 \end{pmatrix},$$
$$v_3^{\psi(2S)} = \begin{pmatrix} -0.481 \\ 0.470 \\ 0.740 \end{pmatrix}, \quad (21)$$

and the corresponding eigenvalues are $\lambda_1^{\psi(2S)} = 4.34$, $\lambda_2^{\psi(2S)} = 4.67 \times 10^{-2}$, and $\lambda_3^{\psi(2S)} = 1.96 \times 10^{-3}$. The eigenvector $v_2^{\psi(2S)}$ is predominantly ${}^1S_0^{[8]}$ and its uncertainty $[(\lambda_2^{\psi(2S)})^{1/2}]$ is fairly small. On the other hand, the eigenvector $v_1^{\psi(2S)}$ has a very large uncertainty $[(\lambda_1^{\psi(2S)})^{1/2}]$. Hence, the ${}^3S_1^{[8]}$ and ${}^3P_0^{[8]}$ LDMEs can vary together in a correlated way that tends to preserve the ${}^1S_0^{[8]}$ dominance. (Recall that the SDCs for these channels have opposite signs.) The eigenvector $v_3^{\psi(2S)}$ has a very small uncertainty $[(\lambda_3^{\psi(2S)})^{1/2}]$ and, therefore, the anticorrelated variation of the ${}^3S_1^{[8]}$ and ${}^3P_0^{[8]}$ LDMEs is highly constrained.

### B. Production of $\chi_{c1}$ and $\chi_{c2}$

We determine the two $\chi_{cJ}$ LDMEs by fitting to ATLAS cross-section data [51]. In order to suppress possible nonfactorizing contributions we fit only to data for which $p_T$ is greater than 11 GeV. We ignore feeddown contributions. The $\psi(2S)$ decays into $\chi_{c1}\gamma$ and $\chi_{c2}\gamma$ with branching ratios of 9.55% and 9.11%, respectively. These contributions amount to only a few percent of the measured cross sections and are much smaller than the theoretical uncertainties.

The fitted LP + NLO $\chi_{c1}$ and $\chi_{c2}$ cross sections are compared with the data in Fig. 11. We do not consider the $\chi_{c0}$ cross section because the $\chi_{c0}$ branching ratio to $J/\psi\gamma$ is small and the corresponding contribution to the prompt $J/\psi$ cross section is negligible. Again, we obtain a good fit to data, with $\chi^2/\text{d.o.f.} = 1.19/8$. The contributions of the individual channels to the prompt-$\chi_{c1}$ and prompt-$\chi_{c2}$ cross sections are shown in Fig. 12. There are substantial cancellations between the contributions of the ${}^3S_1^{[8]}$ and ${}^3P_J^{[1]}$ channels.

The resulting LDMEs are

$$\langle \mathcal{O}^{\chi_c}({}^3S_1^{[8]}) \rangle = (5.74 \pm 1.31) \times 10^{-3}\ \text{GeV}^3, \quad (22a)$$

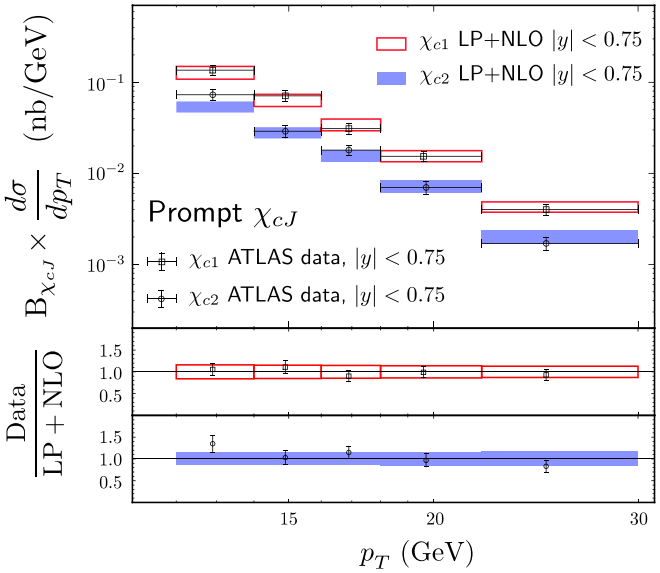


FIG. 11. The differential cross sections for prompt $\chi_{c1}$ and $\chi_{c2}$ production at the LHC ($\sqrt{s} = 7$ TeV). $B_{\chi_{cJ}} = \text{Br}[\chi_{cJ} \to J/\psi + \gamma] \times \text{Br}[J/\psi \to \mu^+\mu^-]$.

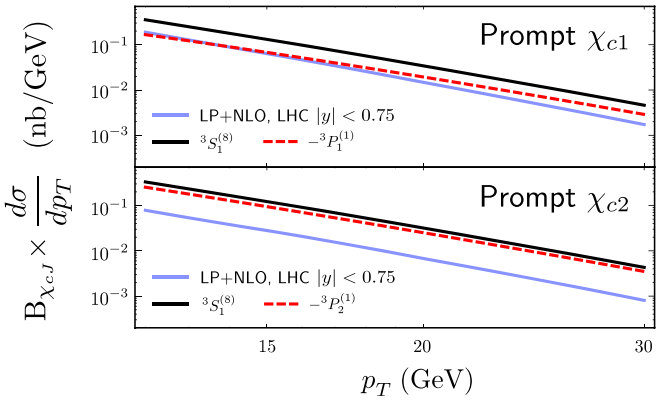


FIG. 12. Contributions of the individual channels to the differential cross sections for prompt $\chi_{c1}$ and $\chi_{c2}$ production at the LHC ($\sqrt{s} = 7$ TeV). $B_{\chi_{cJ}} = \text{Br}[\chi_{cJ} \to J/\psi + \gamma] \times \text{Br}[J/\psi \to \mu^+\mu^-]$.

$$\frac{\langle \mathcal{O}^{\chi_c}({}^3P_0^{[1]}) \rangle}{m_c^2} = (3.53 \pm 1.08) \times 10^{-2}\ \text{GeV}^3. \quad (22b)$$

The correlation matrix of the uncertainties in $\langle \mathcal{O}^{\chi_c}({}^3S_1^{[8]}) \rangle$ and $\langle \mathcal{O}^{\chi_c}({}^3P_0^{[1]}) \rangle / m_c^2$, respectively, is

$$C^{\chi_c} = \begin{pmatrix} 1.71 & 14.0 \\ 14.0 & 117 \end{pmatrix} \times 10^{-6}\ \text{GeV}^6. \quad (23)$$

The relative uncertainties in these LDMEs are fairly small, but there are substantial correlations between them. The correlation matrix of relative uncertainties is

$$\bar{C}^{\chi_c} = \begin{pmatrix} 5.18 & 6.91 \\ 6.91 & 9.39 \end{pmatrix} \times 10^{-2}. \quad (24)$$

The normalized eigenvectors of $\bar{C}^{\chi_c}$ are

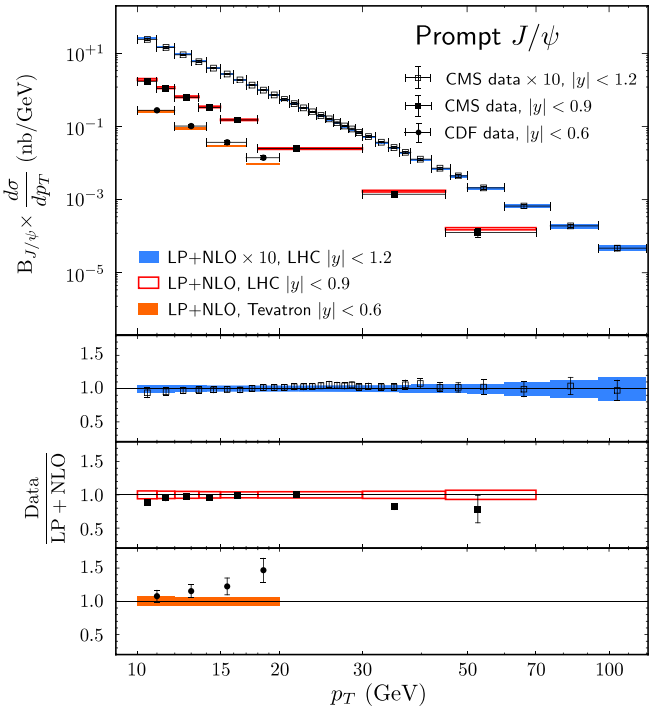


FIG. 13. The differential cross section for prompt $J/\psi$ production at the Tevatron ($\sqrt{s} = 1.96\,\text{TeV}$) and the LHC ($\sqrt{s} = 7\,\text{TeV}$). $B_{J/\psi} = \text{Br}[J/\psi \to \mu^+\mu^-]$.

$$v_1^{\chi_c} = \begin{pmatrix} 0.595 \\ 0.804 \end{pmatrix}, \qquad v_2^{\chi_c} = \begin{pmatrix} 0.804 \\ -0.595 \end{pmatrix}, \tag{25}$$

and the corresponding eigenvalues are $\lambda_1^{\chi_c} = 0.145$ and $\lambda_2^{\chi_c} = 5.70 \times 10^{-4}$. We see that, while the eigenvector $v_1^{\chi_c}$ has a small uncertainty, the ${}^3S_1^{[8]}$ and ${}^3P_0^{[1]}$ LDMEs can vary in a correlated way. However, from the very small uncertainty of the eigenvector $v_2^{\chi_c}$, we see that anticorrelated variation of these LDMEs is highly constrained.

At leading order in $v$, the color-singlet LDME is related to the derivative of the wave function at the origin as

$$\langle \mathcal{O}({}^3P_0^{[1]}) \rangle_{\chi_c} = 2N_c \frac{3}{4\pi} |R'(0)|^2. \tag{26}$$

The value of the color-singlet LDME that we obtained from our fit corresponds to $|R'(0)|^2 = 0.055 \pm 0.017\ \text{GeV}^5$. This is consistent with the value $|R'(0)|^2 = 0.075\ \text{GeV}^5$ that was obtained in Ref. [49] by using the Buchmüller-Tye potential. It is also consistent with the value that was determined in Ref. [52] from the two-photon decay rates of the $\chi_{c0}$ and the $\chi_{c2}$, namely, $\langle \mathcal{O}({}^3P_0^{[1]}) \rangle_{\chi_c} = 0.060^{+0.043}_{-0.029}\ \text{GeV}^5$, which corresponds to $|R'(0)|^2 = 0.042^{+0.030}_{-0.020}\ \text{GeV}^5$.

### C. Production of prompt $J/\psi$

We determine the $J/\psi$ LDMEs by fitting to the CDF [11] and CMS [12,48] prompt-$J/\psi$ cross-section data. In order to suppress possible nonfactorizing contributions, we fit only to data for $p_T$ greater than 10 GeV. We compute the feeddown contributions from the decays of $\psi(2S)$, $\chi_{c1}$, and $\chi_{c2}$ by making use of the LDMEs that were determined in the preceding sections. The prompt-$J/\psi$ cross section is given by

$$\begin{aligned} \frac{d\sigma_{J/\psi}^{\text{prompt}}}{dp_T} = {} & \frac{d\sigma_{J/\psi}^{\text{direct}}}{dp_T} + \frac{d\sigma_{\psi(2S)}}{dp_T^{\psi(2S)}} \text{Br}[\psi(2S) \to J/\psi + X] \\ & + \frac{d\sigma_{\chi_{c1}}}{dp_T^{\chi_{c1}}} \text{Br}[\chi_{c1} \to J/\psi + \gamma] \\ & + \frac{d\sigma_{\chi_{c2}}}{dp_T^{\chi_{c2}}} \text{Br}[\chi_{c2} \to J/\psi + \gamma]. \end{aligned} \tag{27}$$

Here, we ignore the feeddown contribution from the decay of the $\chi_{c0}$. As we have mentioned, the $\chi_{c0}$ decays into $J/\psi\gamma$ with a small branching ratio, and the contribution to the prompt $J/\psi$ cross section is negligible. $p_T$ is the transverse momentum of the $J/\psi$, and $p_T^H$ is the transverse momentum of $H = \psi(2S), \chi_{cJ}$. In the feeddown contributions, we take $p_T^H$ to be

$$p_T^H = \frac{m_H}{m_{J/\psi}} p_T. \tag{28}$$

The relation (28) is derived by neglecting the 3-momentum of the $J/\psi$ in the $H$ rest frame in comparison with $m_{J/\psi}$.[3]

We take the value of the color-singlet LDME that has been obtained from the electromagnetic decay rate [55]: $\langle \mathcal{O}^{J/\psi}({}^3S_1^{[1]}) \rangle = 1.32\ \text{GeV}^3$. Again, the contribution from the color-singlet channel is much smaller than the theoretical uncertainties, ranging from 4% for the bin 10 GeV $< p_T <$ 11 GeV to 0.2% for the bin 95 GeV $< p_T <$ 120 GeV in comparison with the direct $J/\psi$ cross section.

We obtain a good fit to the data, with $\chi^2/\text{d.o.f.} = 8.20/40$. The fitted LP + NLO cross section is shown in comparison with the data in Fig. 13. The contributions of the individual channels to the direct $J/\psi$ cross section are shown in Fig. 14. The direct $J/\psi$ cross section is dominated by the ${}^1S_0^{[8]}$ channel at all values of $p_T$ between 10 GeV and 100 GeV.

[3]We have estimated the effects of corrections to this relation on the contributions of $\chi_{c1}$ and $\chi_{c2}$ feeddown to the $J/\psi$ unpolarized and polarized cross sections. In these estimates, we computed the angular distribution of the $J/\psi$ momentum in the $\chi_{cJ}$ rest frame by making use of the formalism of Ref. [53], and we included the E1, M2, and E3 electromagnetic transition amplitudes, taking the M2 and E3 amplitudes to be given by the central values of the measurement of the CLEO Collaboration [54]. We find that the corrections to the feeddown contributions are no more than 8% in any of the $J/\psi$ polarization channels. Furthermore, the corrections are essentially flat as functions of $p_T$, deviating by only about 1% over the range 10 GeV $\le p_T \le$ 100 GeV, with almost all of the deviation occurring between 10 GeV and 15 GeV. Hence, the corrections have little effect on the shapes of the cross sections and can be absorbed into normalization shifts of the LDMEs of a few percent or less.

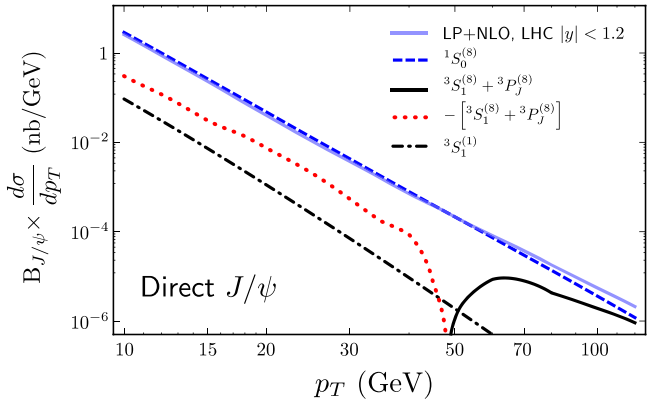


FIG. 14. Contributions of the individual channels to the differential cross section for direct $J/\psi$ production at the LHC ($\sqrt{s} = 7$ TeV). $B_{J/\psi} = \mathrm{Br}[J/\psi \to \mu^+\mu^-]$.

The color-octet LDMEs that are obtained from the fit are

$$\langle \mathcal{O}^{J/\psi}({}^3S_1^{[8]})\rangle = (-7.13 \pm 3.64) \times 10^{-3}\ \mathrm{GeV}^3, \quad (29a)$$

$$\langle \mathcal{O}^{J/\psi}({}^1S_0^{[8]})\rangle = (+1.10 \pm 0.14) \times 10^{-1}\ \mathrm{GeV}^3, \quad (29b)$$

$$\frac{\langle \mathcal{O}^{J/\psi}({}^3P_0^{[8]})\rangle}{m_c^2} = (-3.12 \pm 1.51) \times 10^{-3}\ \mathrm{GeV}^3. \quad (29c)$$

The correlation matrix of the uncertainties in $\langle \mathcal{O}^{J/\psi}({}^3S_1^{[8]})\rangle$, $\langle \mathcal{O}^{J/\psi}({}^1S_0^{[8]})\rangle$, and $\langle \mathcal{O}^{J/\psi}({}^3P_0^{[8]})\rangle/m_c^2$, respectively, is

$$C^{J/\psi} = \begin{pmatrix} 13.3 & -38.2 & 5.48 \\ -38.2 & 188 & -14.6 \\ 5.48 & -14.6 & 2.29 \end{pmatrix} \times 10^{-6}\ \mathrm{GeV}^6. \quad (30)$$

The correlation matrix of relative uncertainties is

$$\bar{C}^{J/\psi} = \begin{pmatrix} 26.1 & 4.88 & 24.7 \\ 4.88 & 1.55 & 4.26 \\ 24.7 & 4.26 & 23.5 \end{pmatrix} \times 10^{-2}. \quad (31)$$

The normalized eigenvectors of $\bar{C}^{J/\psi}$ are

$$v_1^{J/\psi} = \begin{pmatrix} 0.719 \\ 0.131 \\ 0.682 \end{pmatrix}, \quad v_2^{J/\psi} = \begin{pmatrix} 0.168 \\ 0.920 \\ -0.354 \end{pmatrix},$$

$$v_3^{J/\psi} = \begin{pmatrix} -0.674 \\ 0.369 \\ 0.640 \end{pmatrix}, \quad (32)$$

and the corresponding eigenvalues are $\lambda_1^{J/\psi} = 0.504$, $\lambda_2^{J/\psi} = 8.06 \times 10^{-3}$, and $\lambda_3^{J/\psi} = 2.35 \times 10^{-4}$. As is the case for the $\psi(2S)$, the eigenvector that is predominantly $^1S_0^{[8]}$, namely, $v_2^{J/\psi}$, has a fairly small uncertainty. However, the eigenvector $v_1^{J/\psi}$ has a very large uncertainty. Therefore, variations of the $^3S_1^{[8]}$ and $^3P_0^{[8]}$ LDMEs are correlated and tend to preserve the $^1S_0^{[8]}$ dominance. (Recall that the SDCs for these channels have opposite signs.) The very small uncertainty of the eigenvector $v_3^{J/\psi}$ means that the anticorrelated variation of the $^3S_1^{[8]}$ and $^3P_0^{[8]}$ LDMEs is highly constrained.

## VI. PREDICTIONS FROM EXTRACTED LDMEs

In this section, we use the LDMEs that we have extracted from the fits to cross sections to make predictions of cross-section ratios and polarizations. We estimate the uncertainties in these predictions by making use of the eigenvectors and eigenvalues of the LDME uncertainty correlation matrices. In the expression for each prediction, we write the LDMEs in terms of the eigenvectors. Then, we vary each eigenvector about its central value by an amount that is equal to the square root of its eigenvalue. We take the resulting variation in the prediction as the uncertainty in the prediction from variations of that eigenvector. Finally, we estimate the total uncertainty in the prediction by adding the uncertainties from the variations of the individual eigenvectors in quadrature.

### A. Ratios $R_H$

We can use our predictions for the $J/\psi$, $\psi(2S)$, and $\chi_{cJ}$ cross sections and the LDMEs that we have extracted to compute the ratios $R_H$, which are defined by

$$R_H = \frac{\mathrm{Br}[H \to J/\psi + X] \times d\sigma_H/dp_T^H}{d\sigma_{J/\psi}^{\mathrm{prompt}}/dp_T}, \quad (33)$$

where $p_T^H$ is given in Eq. (28). In Figs. 15 and 16 we show our results for $R_{\psi(2S)}$ and $R_{\chi_c} \equiv R_{\chi_{c1}} + R_{\chi_{c2}}$, respectively. As can be seen from Fig. 16, our prediction for $R_{\chi_c}$ lies systematically below the ATLAS [51] and LHCb [56] measurements for $p_T < 15$ GeV. This discrepancy occurs because the prediction for the numerator of $R_{\chi_c}$ lies slightly below the data at low $p_T$, while the prediction for the

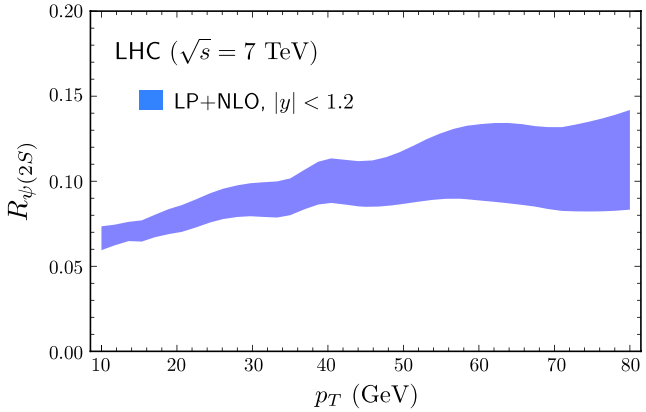


FIG. 15. Fraction of prompt $J/\psi$'s produced in feeddown from $\psi(2S)$ decays at the LHC ($\sqrt{s} = 7$ TeV).

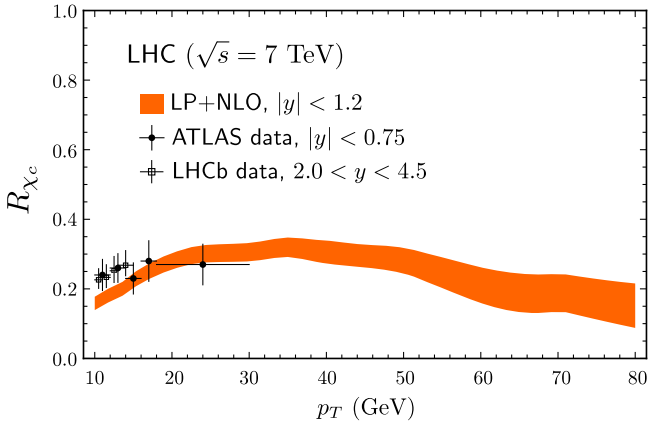


FIG. 16. Fraction of prompt $J/\psi$'s produced in feeddown from $\chi_{c1}$ and $\chi_{c2}$ decays at the LHC ($\sqrt{s} = 7$ TeV).

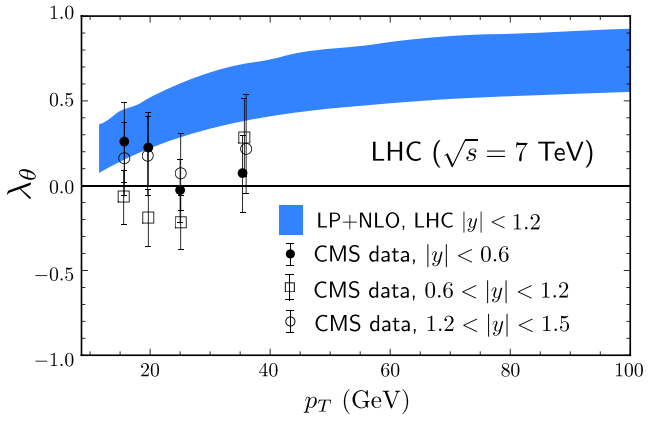


FIG. 17. Polarization of prompt $\psi(2S)$ at the LHC ($\sqrt{s} = 7$ TeV).

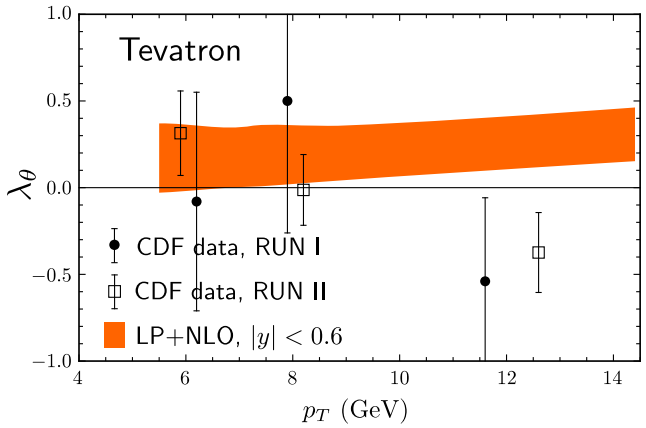


FIG. 18. Polarization of prompt $\psi(2S)$ at the Tevatron ($\sqrt{s} = 1.96$ TeV).

denominator of $R_{\chi_c}$ lies slightly above the data at low $p_T$. However, the predictions for both the numerator and the denominator agree with the data within uncertainties. We also note that corrections to the relation (28) for the $J/\psi$ momentum would increase the theoretical prediction for $R_{\chi_c}$ by a few percent.

### B. Polarization predictions

We now compute prompt-$\psi(2S)$ and prompt-$J/\psi$ polarizations by making use of the LDMEs that we have determined from fits to the cross-section data. We also compute the effects of feeddown from the $\psi(2S)$ and $\chi_{cJ}$ states on the polarizations of the prompt $J/\psi$'s.

For $J = 1$ states, one measure of the polarization is the polarization parameter $\lambda_\theta$, which is defined as

$$\lambda_\theta = \frac{\sigma - 3\sigma_L}{\sigma + \sigma_L}, \tag{34}$$

where $\sigma$ and $\sigma_L$ are the polarization-summed and longitudinal cross sections, respectively. If the $J = 1$ state is completely transversely (longitudinally) polarized, then $\sigma_L = 0$ ($\sigma_L = \sigma$), and $\lambda_\theta = +1$ ($\lambda_\theta = -1$). If the $J = 1$ state is unpolarized, then $\sigma = 3\sigma_L$, and $\lambda_\theta = 0$.

We show the polarization of the $\psi(2S)$ as produced at the LHC at $\sqrt{s} = 7$ TeV and at the Tevatron at $\sqrt{s} = 1.96$ TeV in Figs. 17 and 18, respectively. The prediction for the CMS polarization is in fair agreement with the CMS data [15]. The prediction for the polarization at the Tevatron is in rough agreement with the CDF Run I [13] and Run II [14] data, given the very large error bars. (Although the CDF Run I data were taken at $\sqrt{s} = 1.8$ TeV, rather than at $\sqrt{s} = 1.96$ TeV, this energy shift produces a negligible change in the polarization prediction.) The predicted $\psi(2S)$ polarization grows as $p_T$ increases, owing to the fact that the ${}^1S_0^{[8]}$ channel is no longer dominant at large $p_T$. Hence, measurements of the $\psi(2S)$ polarization at larger values of $p_T$ would provide an important test of the theoretical prediction.

The longitudinal prompt-$J/\psi$ cross section, including the feeddown contributions from the decays of the $\psi(2S)$, the $\chi_{c1}$, and the $\chi_{c2}$ is computed as follows:

$$\begin{aligned}\frac{d\sigma^{\rm prompt}_{J/\psi(\lambda=0)}}{dp_T} = &\frac{d\sigma^{\rm direct}_{J/\psi(\lambda=0)}}{dp_T} + \frac{d\sigma_{\psi(2S)(\lambda=0)}}{dp_T^{\psi(2S)}}{\rm Br}[\psi(2S)\to J/\psi + X] \\ &+ \frac{1}{2}\left(\frac{d\sigma_{\chi_{c1}(\lambda=+1)}}{dp_T^{\chi_{c1}}} + \frac{d\sigma_{\chi_{c1}(\lambda=-1)}}{dp_T^{\chi_{c1}}}\right) \\ &\times {\rm Br}[\chi_{c1}\to J/\psi+\gamma] \\ &+ \left[\frac{2}{3}\frac{d\sigma_{\chi_{c2}(\lambda=0)}}{dp_T^{\chi_{c2}}} + \frac{1}{2}\left(\frac{d\sigma_{\chi_{c2}(\lambda=+1)}}{dp_T^{\chi_{c2}}} + \frac{d\sigma_{\chi_{c2}(\lambda=-1)}}{dp_T^{\chi_{c2}}}\right)\right] \\ &\times {\rm Br}[\chi_{c2}\to J/\psi+\gamma],\end{aligned} \tag{35}$$

where $p_T^H$ is given by Eq. (28). In deriving Eq. (35), we have assumed that the polarization of the $\psi(2S)$ is completely transferred to $J/\psi$ and that the decays $\chi_{cJ} \to J/\psi + \gamma$ proceed through an E1 transition. In the decays $\chi_{cJ} \to J/\psi + \gamma$, the higher multipole corrections are poorly

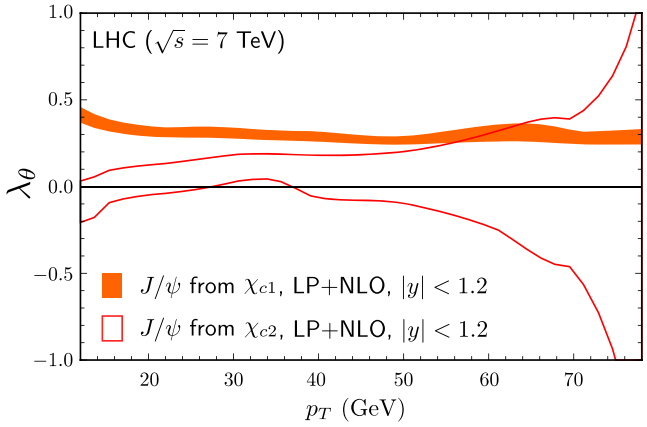


FIG. 19. Polarization of $J/\psi$ from $\chi_{cJ}$ decays at the LHC ($\sqrt{s} = 7$ TeV).

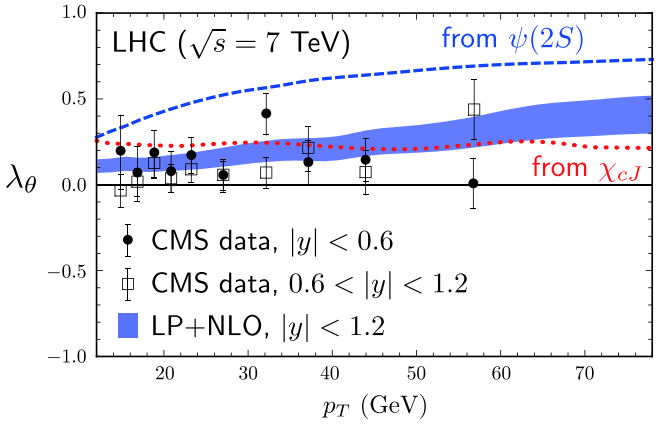


FIG. 20. Polarization of prompt $J/\psi$'s at the LHC ($\sqrt{s} = 7$ TeV). The polarizations of $J/\psi$'s produced in feeddown from the $\psi(2S)$ and the $\chi_{cJ}$ states are shown with dashed and dotted lines, respectively.

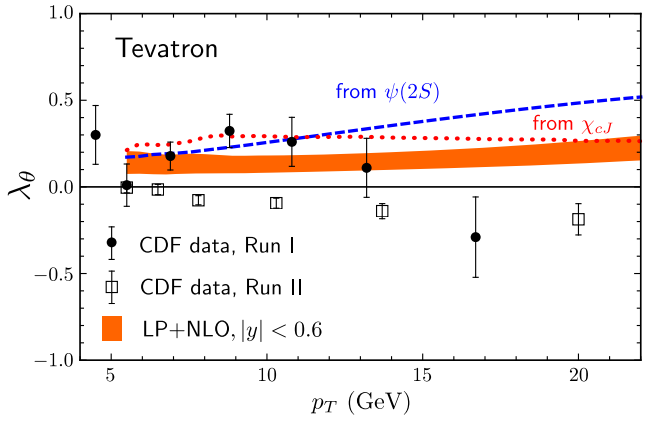


FIG. 21. Polarization of prompt $J/\psi$'s produced at the Tevatron ($\sqrt{s} = 1.96$ TeV). The polarizations of $J/\psi$'s produced in feeddown from the $\psi(2S)$ and the $\chi_{cJ}$ states are shown with dashed and dotted lines, respectively.

known, but they have little effect on the polarizations of the $J/\psi$'s that are produced in $\chi_{cJ}$ decays [53].

We show the polarization of $J/\psi$'s from $\chi_{cJ}$ decays at the LHC at $\sqrt{s} = 7$ TeV in Fig. 19. In Fig. 20, we show the polarization of prompt $J/\psi$'s produced at the LHC at $\sqrt{s} = 7$ TeV, including feeddown from the $\psi(2S)$ and the $\chi_{cJ}$ states. The prediction is in good agreement with the CMS data [15]. Finally, in Fig. 21, we show the polarization of prompt $J/\psi$'s produced at the Tevatron at $\sqrt{s} = 1.96$ TeV, including feeddown from the $\psi(2S)$ and the $\chi_{cJ}$ states. The prediction is in good agreement with the CDF Run I data [13], but disagrees with the CDF Run II data [14]. (Although the CDF Run I data were taken at $\sqrt{s} = 1.8$ TeV, rather than at $\sqrt{s} = 1.96$TeV, this energy shift produces a negligible change in the polarization prediction.) We note that the predicted polarizations are almost the same for the LHC and the Tevatron, while the CDF Run II polarization data lies significantly below the CMS polarization data.

The fairly small polarizations that are seen in the predictions for the prompt $J/\psi$'s and $\psi(2S)$'s are a consequence of the dominance in the production rates of the ${}^1S_0^{[8]}$ channel, which, of course, is completely unpolarized. This mechanism whereby small polarizations can be obtained was noted previously in Refs. [4,25,50].

## VII. SUMMARY AND DISCUSSION

In this paper, we have computed, in the NRQCD factorization framework, leading-power (LP) fragmentation corrections to production of the charmonium states $J/\psi$, $\chi_{cJ}$, and $\psi(2S)$ in $p\bar{p}$ collisions at the Tevatron and in $pp$ collisions at the LHC. Specifically, our calculation makes use of parton production cross sections (PPCSs) through order $\alpha_s^3$ (NLO) and fragmentation functions (FFs) through order $\alpha_s^2$. We have also used the DGLAP equation to resum leading logarithms of $p_T^2/m_c^2$ to all orders in $\alpha_s$. Our calculations take into account the effects of feeddown from the $\psi(2S)$ and $\chi_{cJ}$ states on the prompt-$J/\psi$ cross sections and polarizations. Hence, the work in the present paper is an extension and a refinement of the work in Ref. [25], which also addressed LP corrections, but which did not include computations of cross sections or polarizations for the $\psi(2S)$ or $\chi_{cJ}$ states or include the effects of feeddown from those states. We find that the LP corrections, beyond those that are contained in fixed-order calculations through NLO in $\alpha_s$, are substantial—typically of order 100% at large $p_T$. Owing to a partial cancellation between the LO and NLO contributions in the ${}^3P_J^{[8]}$ channel, the LP corrections have a very significant effect on the shape in that channel.

As was pointed out in Ref. [25], the all-orders resummations of logarithms of $p_T^2/m_c^2$ have only small effects on the predictions for the cross sections and polarizations. Hence, almost all of the large additional LP corrections that we find arise from nonlogarithmic contributions of order $\alpha_s^5$.

Our approach in calculating the LP fragmentation corrections is to use the most accurate results for the PPCSs and FFs that are currently available. This means that we have computed some, but not all, of the LP contributions in order $\alpha_s^5$, i.e., NNLO in terms of the fixed-order calculations. In the case of gluon fragmentation, a complete calculation of the order-$\alpha_s^5$ contributions in the ${}^1S_0^{[8]}$ and ${}^3P_J^{[8]}$ channels would require the calculation of the NLO corrections to the FFs for those channels. In the case of gluon fragmentation, a complete calculation of the order-$\alpha_s^5$ contributions in the ${}^3S_1^{[8]}$ channel would require a calculation of the NNLO corrections to the FFs for that channel and the NNLO corrections to the PPCSs. We expect these uncalculated LP corrections in order $\alpha_s^5$ to be of comparable size, in each channel, to the LP corrections that we have calculated in this paper. Hence, the actual theoretical uncertainties may be much larger than the estimates that we have obtained by varying the scales $\mu_r$ and $\mu_f$. However, we emphasize that the calculation in this paper eliminates the largest existing source of theoretical uncertainty by taking into account leading logarithms of $p_T^2/m_c^2$ at all orders in $\alpha_s$.

We have combined the LP corrections that we have calculated with the NLO fixed-order calculations from Refs. [1,3,4] to obtain predictions for the production cross sections and polarizations as functions of $p_T$. By fitting the cross-section predictions to the Tevatron and LHC cross-section data, we have obtained values for the NRQCD nonperturbative long-distance matrix elements (LDMEs) that enter into the production predictions through order $v^4$. Since the LP approximation is valid only for $p_T \gg m_H$, where $m_H$ is the quarkonium mass, we use only data for which $p_T$ is greater than $3m_H$. We obtain good fits to the high-$p_T$ cross sections, with $\chi^2/\text{d.o.f.} \ll 1$ in each case.

One interesting result of the fits to the $\chi_{cJ}$ cross sections is that the value of the ${}^3P_0^{[1]}$ LDME that we obtain is in good agreement with the value that has been obtained in a potential model and with values that have been extracted from the two-photon decays of the $\chi_{c0}$ and $\chi_{c2}$. This agreement of values of the ${}^3P_0^{[1]}$ LDME that have been obtained through very different methods is important evidence in support of the NRQCD factorization conjecture. We note that, in previous works on the $\chi_{cJ}$ cross section, which were based on fixed-order NLO calculations, the ${}^3P_0^{[1]}$ LDME was fixed to values that were obtained from potential models [6,57–61].

We have used our cross-section predictions to predict the ratio $R_{\chi_c}$, which is the $\chi_{cJ}$ feeddown contribution to the prompt-$J/\psi$ cross section divided by the prompt-$J/\psi$ cross section itself. The prediction lies systematically below the data for $p_T < 15$ GeV. This discrepancy in $R_{\chi_c}$ seems to be the result of a downward deviation in the numerator combined with an upward deviation in the denominator. However, the predictions for both numerator and the denominator agree with the data within uncertainties.

We have also used the extracted LDMEs to predict the $J/\psi$, $\psi(2S)$, and $\chi_{cJ}$ polarizations. The predictions for the $J/\psi$ polarizations agree with the CMS data and the CDF Run I data, but lie systematically above the CDF Run II data. The CDF Run I data show a slightly longitudinal polarization, while the CMS data show a slightly transverse polarization. However, the theoretical predictions are very similar for the CDF and CMS kinematics. The predictions for the $\psi(2S)$ polarizations agree with the Tevatron data and the LHC data, although the theoretical and experimental uncertainties are quite large. For $\psi(2S)$ production, the ${}^1S_0^{[8]}$ channel is no longer dominant at large $p_T$, and, so, the predicted $\psi(2S)$ polarization becomes more transverse as $p_T$ increases. It is important to test this prediction through measurements of the $\psi(2S)$ polarization with good precision at larger values of $p_T$. There are, as yet, no measurements of the $\chi_{cJ}$ polarizations. These would also provide very useful tests of the theoretical predictions.

While we have obtained a reasonably good description of the hadroproduction cross sections and polarizations for the $J/\psi$, $\psi(2S)$, and $\chi_{cJ}$ states, our results do not address two outstanding problems in quarkonium production, namely, the HERA $J/\psi$ photoproduction cross section, as measured by the H1 Collaboration [16,17], and the $\eta_c$ hadroproduction cross section, as measured by the LHCb Collaboration [20]. In the case of the $J/\psi$ photoproduction cross section, additional LP fragmentation corrections, analogous to those that were computed in this paper, were computed in Ref. [62]. Those additional LP corrections have very small effects on the photoproduction cross section. For the choices of LDMEs that were used in Ref. [62], the theoretical prediction for the photoproduction cross section is dominated by the contribution from the ${}^1S_0^{[8]}$ channel. The value for $\langle \mathcal{O}^{J/\psi}({}^1S_0^{[8]}) \rangle$ in Eq. (29) is about 10% larger than the value from Ref. [25], which was used in Ref. [62]. Hence, it makes the discrepancy between theory and experiment slightly worse. In the case of the $\eta_c$ cross section, the change in value of $\langle \mathcal{O}^{J/\psi}({}^1S_0^{[8]}) \rangle$ from Ref. [25] to the present paper also makes the discrepancy between theory and experiment slightly worse.

While there remain important discrepancies between theory and experiment in quarkonium production at high $p_T$, the theoretical predictions are far from settled. At a minimum, a complete calculation of all of the LP contributions in order $\alpha_s^5$ is needed in order to have reasonable control of the theoretical uncertainties. These LP contributions in order $\alpha_s^5$ may be most important in the ${}^3P_J^{[8]}$ channel because of their greater potential to affect the shape in that channel. Higher-order calculations of NLP contributions may also be needed, especially in the ${}^1S_0^{[8]}$ channel, for which the LP contributions are not dominant until very large values of $p_T$. New measurements at the LHC of the

$\psi(nS)$, $\chi_{cJ}$, $\Upsilon(nS)$, and $\chi_{bJ}$ cross sections and polarizations and the $\eta_c$ cross section, all at unprecedentedly large values of $p_T$, can provide definitive tests of the improved theoretical predictions.

## ACKNOWLEDGMENTS

We thank Jean-Philippe Guillet for providing information about the computer code that implements the NLO parton-scattering results of Ref. [30]. The work of G. T. B. and H. S. C. is supported by the U.S. Department of Energy, Division of High Energy Physics, under Contract No. DE-AC02-06CH11357. The work of K.-T. C. and Y.-Q. M. is supported in part by the National Natural Science Foundation of China (Grants No. 11475005 and No. 11075002). J. L. thanks the Korean Future Collider Working Group for enjoyable discussions regarding the work presented here. The work of J. L. and U-R. K. was supported by the Do-Yak project of National Research Foundation of Korea funded by the Korea government (MSIP) under Contract No. NRF-2015R1A2A1A15054533. The submitted manuscript has been created in part by UChicago Argonne, LLC, Operator of Argonne National Laboratory. Argonne, a U.S. Department of Energy Office of Science laboratory, is operated under Contract No. DE-AC02-06CH11357.

## APPENDIX: NUMERICAL TREATMENT OF DIVERGENCES IN FRAGMENTATION FUNCTIONS

The LP-factorization contribution to the cross section is given by the convolution of the PPCSs $d\hat{\sigma}_{AB\to i+X}/dp_T$ and the FFs $D_{i\to Q\bar{Q}(n)}(z,\mu_f)$:

$$\frac{d\sigma^{\rm LP}_{AB\to Q\bar{Q}(n)+X}}{dp_T}=\int_{z_0}^1 dz\,\frac{d\hat{\sigma}_{AB\to i+X}(z,\mu_f)}{dp_T}D_{i\to Q\bar{Q}(n)}(z,\mu_f). \tag{A1}$$

Here, $z_0=\frac{p_T}{\sqrt{s}}(e^{+y}+e^{-y})$. We compute the evolved FFs by solving the LO DGLAP equation in Mellin space (moment space) and performing the inverse Mellin transform numerically. As is discussed in Sec. III C, the inverse Mellin transform becomes numerically unstable near $z=1$ because $D_{i\to Q\bar{Q}(n)}(z,\mu_f)$ can vary rapidly in this region and may even diverge at $z=1$.

In order to deal with this problem, we partition the integral over $z$ as follows:

$$\begin{aligned}\int_{z_0}^1 dz\,\frac{d\hat{\sigma}_{AB\to i+X}(z,\mu_f)}{dp_T}D_{i\to Q\bar{Q}(n)}(z,\mu_f)&=\int_{z_0}^{1-\epsilon} dz\,\frac{d\hat{\sigma}_{AB\to i+X}(z,\mu_f)}{dp_T}D_{i\to Q\bar{Q}(n)}(z,\mu_f)\\&\quad+\int_{1-\epsilon}^1 dz\,\frac{d\hat{\sigma}_{AB\to i+X}(z,\mu_f)}{dp_T}D_{i\to Q\bar{Q}(n)}(z,\mu_f),\end{aligned} \tag{A2}$$

where $\epsilon$ is a small, positive number that is chosen so that the evolved FF $D_{i\to Q\bar{Q}(n)}(z,\mu_f)$ can be computed reliably for $z<1-\epsilon$. In order to compute the integral over $1-\epsilon<z<1$, we use the fact that the PPCSs behave as $d\hat{\sigma}_{AB\to i+X}/dp_T\sim z^N$ for $z\approx 1$, where $N\approx 4$. Hence, we have

$$\begin{aligned}&\int_{1-\epsilon}^1 dz\,\frac{d\hat{\sigma}_{AB\to i+X}(z,\mu_f)}{dp_T}D_{i\to Q\bar{Q}(n)}(z,\mu_f)\\&=\int_{1-\epsilon}^1 dz\left[\frac{d\hat{\sigma}_{AB\to i+X}(z,\mu_f)}{dp_T}z^{-N}\right][z^N D_{i\to Q\bar{Q}(n)}(z,\mu_f)]\\&\approx\left[\frac{d\hat{\sigma}_{AB\to i+X}(z,\mu_f)}{dp_T}\right]_{z=1}\times\int_{1-\epsilon}^1 dz\,z^N D_{i\to Q\bar{Q}(n)}(z,\mu_f)\\&=\left[\frac{d\hat{\sigma}_{AB\to i+X}(z,\mu_f)}{dp_T}\right]_{z=1}\times\left[\int_0^1 dz\,z^N D_{i\to Q\bar{Q}(n)}(z,\mu_f)-\int_0^{1-\epsilon} dz\,z^N D_{i\to Q\bar{Q}(n)}(z,\mu_f)\right]\\&=\left[\frac{d\hat{\sigma}_{AB\to i+X}(z,\mu_f)}{dp_T}\right]_{z=1}\times\left[\tilde{D}_{i\to Q\bar{Q}(n)}(N+1,\mu_f)-\int_0^{1-\epsilon} dz\,z^N D_{i\to Q\bar{Q}(n)}(z,\mu_f)\right],\end{aligned} \tag{A3}$$

where we have expanded $z^{-N}d\hat{\sigma}_{AB\to i+X}/dp_T$ in powers of $1-z$ and retained only the leading-order contribution, which is simply the value of $d\hat{\sigma}_{AB\to i+X}/dp_T$ at $z=1$. The quantity $\tilde{D}_{i\to Q\bar{Q}(n)}(N+1,\mu_f)$, the $(N+1)$st moment of $D_{i\to Q\bar{Q}(n)}$, is known analytically, and the integral over the range $0<z<1-\epsilon$ can be computed numerically. Hence, in our calculations, we use the expression

$$\int_{z_0}^{1} dz \frac{d\hat{\sigma}_{AB\to i+X}(z,\mu_f)}{dp_T} D_{i\to Q\bar{Q}(n)}(z,\mu_f)$$
$$\approx \int_{z_0}^{1-\epsilon} dz \frac{d\hat{\sigma}_{AB\to i+X}(z,\mu_f)}{dp_T} D_{i\to Q\bar{Q}(n)}(z,\mu_f)$$
$$+ \left[\frac{d\hat{\sigma}_{AB\to i+X}(z,\mu_f)}{dp_T}\right]_{z=1}$$
$$\times \left[\tilde{D}_{i\to Q\bar{Q}(n)}(N+1,\mu_f) - \int_0^{1-\epsilon} dz\, z^N D_{i\to Q\bar{Q}(n)}(z,\mu_f)\right]. \tag{A4}$$

In our numerical calculations, we take $N = 4$ and $\epsilon = 10^{-6}$. We have varied $N$ between 3.1 and 7 and find that the largest sensitivity to $N$ occurs at low $p_T$ and is less than $3 \times 10^{-6}$ of the contribution in each channel.

We have compared numerical results from Eq. (A4) for $\mu_f$ near $\mu_0$ with the analytic expression for the evolved FFs through second order in $\alpha_s$. The results agree to better than 1%. We expect numerical difficulties in Eq. (A4) to be most severe as $\mu_f$ approaches $\mu_0$, where the evolved FFs approximate the initial FFs, which, in some cases, are distributions at $z = 1$. Hence, good agreement with the analytic expressions in this region gives us confidence that the algorithm that is based on Eq. (A4) is reliable.


[1] Y.-Q. Ma, K. Wang, and K.-T. Chao, Complete NLO calculation of the $J/\psi$ and $\psi'$ production at hadron colliders, Phys. Rev. D **84**, 114001 (2011).

[2] M. Butenschoen and B. A. Kniehl, Reconciling $J/\psi$ Production at HERA, RHIC, Tevatron, and LHC with NRQCD Factorization at Next-to-Leading Order, Phys. Rev. Lett. **106**, 022003 (2011).

[3] Y.-Q. Ma, K. Wang, and K.-T. Chao, $J/\psi(\psi')$ Production at the Tevatron and the LHC at $\mathcal{O}(\alpha_s^4 v^4)$ in Nonrelativistic QCD, Phys. Rev. Lett. **106**, 042002 (2011).

[4] K.-T. Chao, Y.-Q. Ma, H.-S. Shao, K. Wang, and Y.-J. Zhang, $J/\psi$ Polarization at Hadron Colliders in Nonrelativistic QCD, Phys. Rev. Lett. **108**, 242004 (2012).

[5] M. Butenschoen and B. A. Kniehl, $J/\psi$ Polarization at the Tevatron and the LHC: Nonrelativistic-QCD Factorization at the Crossroads, Phys. Rev. Lett. **108**, 172002 (2012).

[6] B. Gong, L.-P. Wan, J.-X. Wang, and H.-F. Zhang, Polarization for Prompt $J/\psi$ and $\psi(2S)$ Production at the Tevatron and LHC, Phys. Rev. Lett. **110**, 042002 (2013).

[7] M. Butenschoen and B. A. Kniehl, World data of $J/\psi$ production consolidate nonrelativistic QCD factorization at next-to-leading order, Phys. Rev. D **84**, 051501 (2011).

[8] M. Butenschoen and B. A. Kniehl, Complete Next-to-Leading-Order Corrections to $J/\psi$ Photoproduction in Nonrelativistic Quantum Chromodynamics, Phys. Rev. Lett. **104**, 072001 (2010).

[9] M. Butenschoen and B. A. Kniehl, Probing Nonrelativistic QCD Factorization in Polarized $J/\psi$ Photoproduction at Next-to-Leading Order, Phys. Rev. Lett. **107**, 232001 (2011).

[10] G. T. Bodwin, E. Braaten, and G. P. Lepage, Rigorous QCD analysis of inclusive annihilation and production of heavy quarkonium, Phys. Rev. D **51**, 1125 (1995); **55**, 5853(E) (1997).

[11] D. Acosta *et al.* (CDF Collaboration), Measurement of the $J/\psi$ meson and $b-$hadron production cross sections in $p\bar{p}$ collisions at $\sqrt{s} = 1960$ GeV, Phys. Rev. D **71**, 032001 (2005).

[12] S. Chatrchyan *et al.* (CMS Collaboration), $J/\psi$ and $\psi(2S)$ production in $pp$ collisions at $\sqrt{s} = 7$ TeV, J. High Energy Phys. 02 (2012) 011.

[13] T. Affolder *et al.* (CDF Collaboration), Measurement of $J/\psi$ and $\psi(2S)$ Polarization in $p\bar{p}$ Collisions at $\sqrt{s} = 1.8$ TeV, Phys. Rev. Lett. **85**, 2886 (2000).

[14] A. Abulencia *et al.* (CDF Collaboration), Polarization of $J/\psi$ and $\psi(2S)$ Mesons Produced in $p\bar{p}$ Collisions at $\sqrt{s} = 1.96$ TeV, Phys. Rev. Lett. **99**, 132001 (2007).

[15] S. Chatrchyan *et al.* (CMS Collaboration), Measurement of the prompt $J/\psi$ and $\psi(2S)$ polarizations in $pp$ collisions at $\sqrt{s} = 7$ TeV, Phys. Lett. B **727**, 381 (2013).

[16] C. Adloff *et al.* (H1 Collaboration), Inelastic photoproduction of $J/\psi$ mesons at HERA, Eur. Phys. J. C **25**, 25 (2002).

[17] F. D. Aaron *et al.* (H1 Collaboration), Inelastic production of $J/\psi$ mesons in photoproduction and deep inelastic scattering at HERA, Eur. Phys. J. C **68**, 401 (2010).

[18] M. Butenschoen and B. A. Kniehl, Next-to-leading-order tests of non-relativistic-QCD factorization with $J/\psi$ yield and polarization, Mod. Phys. Lett. A **28**, 1350027 (2013).

[19] M. Butenschoen, Z.-G. He, and B. A. Kniehl, $\eta_c$ Production at the LHC Challenges Nonrelativistic QCD Factorization, Phys. Rev. Lett. **114**, 092004 (2015).

[20] R. Aaij *et al.* (LHCb Collaboration), Measurement of the $\eta_c(1S)$ production cross-section in proton-proton collisions via the decay $\eta_c(1S) \to p\bar{p}$, Eur. Phys. J. C **75**, 311 (2015).

[21] H. Han, Y.-Q. Ma, C. Meng, H.-S. Shao, and K.-T. Chao, $\eta_c$ Production at LHC and Implications for the Understanding of $J/\psi$ Production, Phys. Rev. Lett. **114**, 092005 (2015).

[22] H.-F. Zhang, Z. Sun, W.-L. Sang, and R. Li, Impact of $\eta_c$ Hadroproduction Data on Charmonium Production and Polarization within the Nonrelativistic QCD Framework, Phys. Rev. Lett. **114**, 092006 (2015).

[23] J. C. Collins and D. E. Soper, Parton distribution and decay functions, Nucl. Phys. **B194**, 445 (1982).

[24] Z.-B. Kang, J.-W. Qiu, and G. Sterman, Heavy Quarkonium Production and Polarization, Phys. Rev. Lett. **108**, 102002 (2012).

[25] G. T. Bodwin, H. S. Chung, U-R. Kim, and J. Lee, Fragmentation Contributions to $J/\psi$ Production at the Tevatron and the LHC, Phys. Rev. Lett. **113**, 022001 (2014).

[26] V. N. Gribov and L. N. Lipatov, Deep inelastic $ep$ scattering in perturbation theory, Yad. Fiz. **15**, 781 (1972) [Sov. J. Nucl. Phys. **15**, 438 (1972)].
[27] L. N. Lipatov, The parton model and perturbation theory, Yad. Fiz. **20**, 181 (1974) [Sov. J. Nucl. Phys. **20**, 94 (1975)].
[28] Y. L. Dokshitzer, Calculation of the structure functions for deep inelastic scattering and $e^+e^-$ annihilation by perturbation theory in quantum chromodynamics, Zh. Eksp. Teor. Fiz. **73**, 1216 (1977) [Sov. Phys. JETP **46**, 641 (1977)].
[29] G. Altarelli and G. Parisi, Asymptotic freedom in parton language, Nucl. Phys. **B126**, 298 (1977).
[30] F. Aversa, P. Chiappetta, M. Greco, and J. P. Guillet, QCD corrections to parton-parton scattering processes, Nucl. Phys. **B327**, 105 (1989).
[31] B. Jager, A. Schafer, M. Stratmann, and W. Vogelsang, Next-to-leading order QCD corrections to high $p_T$ pion production in longitudinally polarized $pp$ collisions, Phys. Rev. D **67**, 054005 (2003).
[32] Y.-Q. Ma, J.-W. Qiu, and H. Zhang, Heavy quarkonium fragmentation functions from a heavy quark pair. I. $S$ wave, Phys. Rev. D **89**, 094029 (2014).
[33] Y.-Q. Ma, J.-W. Qiu, and H. Zhang, Fragmentation functions of polarized heavy quarkonium, J. High Energy Phys. 06 (2015) 021.
[34] E. Braaten and T. C. Yuan, Gluon fragmentation into $P$-wave heavy quarkonium, Phys. Rev. D **50**, 3176 (1994).
[35] E. Braaten and J. Lee, Next-to-leading order calculation of the color-octet $^3S_1$ gluon fragmentation function for heavy quarkonium, Nucl. Phys. **B586**, 427 (2000).
[36] E. Braaten and Y.-Q. Chen, Dimensional regularization in quarkonium calculations, Phys. Rev. D **55**, 2693 (1997).
[37] G. T. Bodwin, U-R. Kim, and J. Lee, Higher-order relativistic corrections to gluon fragmentation into spin-triplet $S$-wave quarkonium, J. High Energy Phys. 11 (2012) 020.
[38] P. Cho, M. B. Wise, and S. P. Trivedi, Gluon fragmentation into polarized charmonium, Phys. Rev. D **51**, R2039 (1995).
[39] G. T. Bodwin, H. S. Chung, U-R. Kim, and J. Lee, Quark fragmentation into spin-triplet $S$-wave quarkonium, Phys. Rev. D **91**, 074013 (2015).
[40] J. P. Ma, Quark fragmentation into $^3P_J$ quarkonium, Phys. Rev. D **53**, 1185 (1996).
[41] H. Zhang, Ph.D. thesis, Stony Brook University, 2014; http://graduate.physics.sunysb.edu/announ/theses/zhang-hong-august-2014.pdf.
[42] T. C. Yuan, Perturbative QCD fragmentation functions for production of $P$-wave mesons with charm and beauty, Phys. Rev. D **50**, 5664 (1994).
[43] E. Braaten, K. Cheung, and T. C. Yuan, $Z^0$ decay into charmonium via charm quark fragmentation, Phys. Rev. D **48**, 4230 (1993).
[44] E. Braaten and T. C. Yuan, Gluon fragmentation into heavy quarkonium, Phys. Rev. Lett. **71**, 1673 (1993).
[45] E. Braaten and T. C. Yuan, Gluon fragmentation into spin-triplet $S$-wave quarkonium, Phys. Rev. D **52**, 6627 (1995).
[46] Y.-Q. Ma, J.-W. Qiu, G. Sterman, and H. Zhang, Factorized Power Expansion for High-$p_T$ Heavy Quarkonium Production, Phys. Rev. Lett. **113**, 142002 (2014).
[47] T. Aaltonen *et al.* (CDF Collaboration), Production of $\psi(2S)$ mesons in $p\bar{p}$ collisions at 1.96 TeV, Phys. Rev. D **80**, 031103 (2009).
[48] V. Khachatryan *et al.* (CMS Collaboration), Measurement of $J/\psi$ and $\psi(2S)$ Prompt Double-Differential Cross Sections in $pp$ Collisions at $\sqrt{s} = 7$ TeV, Phys. Rev. Lett. **114**, 191802 (2015).
[49] E. J. Eichten and C. Quigg, Quarkonium wave functions at the origin, Phys. Rev. D **52**, 1726 (1995).
[50] P. Faccioli, V. Knünz, C. Lourenço, J. Seixas, and H. K. Wöhri, Quarkonium production in the LHC era: A polarized perspective, Phys. Lett. B **736**, 98 (2014).
[51] G. Aad *et al.* (ATLAS Collaboration), Measurement of $\chi_{c1}$ and $\chi_{c2}$ production with $\sqrt{s} = 7$ TeV $pp$ collisions at ATLAS, J. High Energy Phys. 07 (2014) 154.
[52] H. S. Chung, J. Lee, and C. Yu, Exclusive heavy quarkonium + $\gamma$ production from $e^+e^-$ annihilation into a virtual photon, Phys. Rev. D **78**, 074022 (2008).
[53] P. Faccioli, C. Lourenço, J. Seixas, and H. K. Wöhri, Determination of $\chi_c$ and $\chi_b$ polarizations from dilepton angular distributions in radiative decays, Phys. Rev. D **83**, 096001 (2011).
[54] M. Artuso *et al.* (CLEO Collaboration), Higher-order multipole amplitudes in charmonium radiative transitions, Phys. Rev. D **80**, 112003 (2009).
[55] G. T. Bodwin, H. S. Chung, D. Kang, J. Lee, and C. Yu, Improved determination of color-singlet nonrelativistic QCD matrix elements for $S$-wave charmonium, Phys. Rev. D **77**, 094017 (2008).
[56] R. Aaij *et al.* (LHCb Collaboration), Measurement of the ratio of prompt $\chi_c$ to $J/\psi$ production in $pp$ collisions at $\sqrt{s} = 7$ TeV, Phys. Lett. B **718**, 431 (2012).
[57] Y.-Q. Ma, K. Wang, and K.-T. Chao, QCD radiative corrections to $\chi_{cJ}$ production at hadron colliders, Phys. Rev. D **83**, 111503 (2011).
[58] D. Li, Y.-Q. Ma, and K.-T. Chao, $\chi_{cJ}$ production associated with a $c\bar{c}$ pair at hadron colliders, Phys. Rev. D **83**, 114037 (2011).
[59] H.-S. Shao, Y.-Q. Ma, K. Wang, and K.-T. Chao, Polarizations of $\chi_{c1}$ and $\chi_{c2}$ in Prompt Production at the LHC, Phys. Rev. Lett. **112**, 182003 (2014).
[60] L. Jia, L. Yu, and H.-F. Zhang, A global analysis of the experimental data on $\chi_c$ meson hadroproduction, arXiv:1410.4032.
[61] H.-S. Shao, H. Han, Y.-Q. Ma, C. Meng, Y.-J. Zhang, and K.-T. Chao, Yields and polarizations of prompt $J/\psi$ and $\psi(2S)$ production in hadronic collisions, J. High Energy Phys. 05 (2015) 103.
[62] G. T. Bodwin, H. S. Chung, U-R. Kim, and J. Lee, Fragmentation contributions to $J/\psi$ photoproduction at HERA, Phys. Rev. D **92**, 074042 (2015).